

Syracuse University

SURFACE

Theses - ALL

August 2018

Non-uniform glacial erosion in New York State viewed through the lens of cosmogenic nuclide concentrations and forward modeling

Jennifer Nita Nair
Syracuse University

Follow this and additional works at: <https://surface.syr.edu/thesis>



Part of the [Physical Sciences and Mathematics Commons](#)

Recommended Citation

Nair, Jennifer Nita, "Non-uniform glacial erosion in New York State viewed through the lens of cosmogenic nuclide concentrations and forward modeling" (2018). *Theses - ALL*. 268.

<https://surface.syr.edu/thesis/268>

This is brought to you for free and open access by SURFACE. It has been accepted for inclusion in Theses - ALL by an authorized administrator of SURFACE. For more information, please contact surface@syr.edu.

Abstract

Throughout the Pleistocene the northern hemisphere was subject to alternating ice-free and ice accumulation periods. Today's glacial landscapes, composed of a mix of erosive and depositional geomorphological features, reflect the integrated impacts of successive Pleistocene glaciations. In North America such impacts include the formation of the Great Lakes, the reorganization of river networks and the deposition of till sheets, erratic boulders, and moraines. Nearly all of New York State was covered by ice; however, the impact of the successive glaciations on the landscape varies throughout the state. An examination of the regional topography reveals relatively undissected, streamlined landforms of the Finger Lakes area, while adjacent areas retain a largely remnant dissected fluvial landscape. This variation implies differences in the erosive effect of glaciers on modifying the landscape and this study explores that variation. The earliest work in the area hypothesized that the first glacial episode exploited the differences in rock competence related to the facies of the Appalachian Basin in order to create today's physiographic differences, preparing a path for subsequent advances to follow with no further erosion. This study uses the cosmogenic nuclide ^{10}Be to constrain the magnitude of glacial erosion in the Finger Lakes and adjacent areas. Exploiting a stratigraphically continuous sandstone layer, the Devonian Oriskany Sandstone, an estimate of the amount of glacial erosion experienced by the landscape over the last million years is determined using the concentration ^{10}Be produced at depth by the muon production mechanism. This thesis explores a family of plausible erosion scenarios by forward modeling of the accumulation of ^{10}Be concentrations as successive glacial erosion events exhumed the sandstone layer towards the surface. The model output as well as calculated erosion rates and effective ages are used to make determinations about each of the sites in the context of elevation and topography, including interpretations based on the presence of various glacial erosive features. In an east - west transect across the Finger Lakes Region, increasing site elevation correlates with older effective ages and low erosion rates, with one exception whose high elevation is secondary to its proximity to areas of focused glacial erosion.

**Non-uniform glacial erosion in New York State viewed through the lens of
cosmogenic nuclide concentrations and forward modeling**

By

Jennifer Nair

B.S. Emory University, 2014

Thesis

Submitted in partial fulfillment of the requirements for the degree of
Master of Science in Earth Sciences

Syracuse University
August 2018

Copyright © Jennifer Nair 2018

All Rights Reserved

Acknowledgements

This Master's Thesis aims to better understand the glacial history of Central New York. The help and support of many people and groups both at Syracuse University and outside of academia was integral to the completion of this research. I must begin by wholeheartedly thanking my friends and family for their support. The importance of the support and encouragement I received from my peers, the faculty, and staff within the Earth Science Department at Syracuse University cannot be understated. I would like to thank the Earth Surface and Tectonics Research group starting with Greg Hoke, my advisor, whose insights and guidance were invaluable over the last three years. In addition, the scientific discussions and advice provided by present and former graduate students, Greg Wissink, Pedro Val, JR Slosson, and Nicolas Perez Consuegra, helped me develop my thesis. At the University of Vermont, I would like to thank Paul Bierman and Lee Corbett for the final processing of my cosmogenic nuclide samples. I would also like to thank Paul Bierman and Christa Kelleher as members of my thesis committee whose edits helped me cross the finish line. For allowing me access to and providing information about my sampling sites, I thank Franz Peters at Hanson Aggregates as well as the Seneca Stone Quarry. Finally, I must acknowledge the funding sources which made this project possible. More specifically I would like to thank the Nelson and Prucha Research Funds in support of graduate student research in the Department of Earth Science and NSF Grant EAR-1463709.

Table of Contents

Introduction.....	1
Regional Setting	
Bedrock geology.....	2
Pleistocene glaciations.....	3
Cosmogenic Nuclides.....	5
Methods	
Sampling.....	6
Surface reconstruction.....	7
Sample processing.....	7
Modeling glacial erosion.....	8
Results	
Cosmogenic nuclide concentrations.....	10
Mean erosion rates and effective ages.....	11
Glacial erosion modeling.....	11
Discussion	
Data interpretation.....	12
Limitations of modeling.....	16
Conclusions.....	17
Figures.....	19-26
Tables.....	27-28
Appendix	
A1. Determining sample depth below the surface.....	29-30
A2. Sample processing.....	31-33
A3. Matlab forward modeling script.....	34-43
References.....	44-50
Curriculum Vitae.....	51

List of Figures

Figure 1	
Regional Overview.....	19
Figure 2	
Topographic map of the Study Area.....	20
Figure 3	
Stratigraphic Column.....	21
Figure 4	
Conceptual Model Diagram.....	22
Figure 5	
Example Model Output.....	23
Figure 6	
Summary of Model Outputs.....	24
Figure 7	
Plot of Age and Erosion rate vs. Longitude.....	25
Figure 8	
Swath Profiles.....	26
A1. Figure 1	
Laser Range Finder Diagram.....	30
A2. Figure 2	
Lab Protocols Flowchart.....	32

List of Tables

Table 1	
Sample Data.....	27
Table 2	
Model Parameters.....	28
A1. Table 1	
Historic USGS Topographic Map Details.....	30
A2. Table 2	
Syracuse University Sample Processing.....	32
A2. Table 3	
1 st Quartz Purity Results.....	33
A2. Table 4	
2 nd Quartz Purity Results.....	33

Introduction

The periodic advance and retreat of continental ice sheets in the northern hemisphere has been a persistent feature of the Earth's climate system since the Pliocene (Paillard, 1998). Glaciers leave a suite of readily recognizable erosive and depositional landforms in their wake such as U-shaped valleys, nunataks, moraines, and glacial erratics (von Engel, 1961; Anderson and Anderson, 2010). Since ice sheets, with the exception of nunataks, completely cover and flow over the land surface, modifying the landforms of prior glaciations, the record of the last glacial maximum (LGM) deglaciation dominates our view of glacial erosion and deposition (MacClintock and Apfel 1944; Fullerton, 1986; Muller and Calkin, 1993). It is often difficult to definitively ascribe the erosion and sculpting of the bedrock as the result of a single or integrated number of glacial events given the general challenges of directly dating landforms (Davis et al., 1999), let alone in glaciated terranes (e.g. Stroeven et al., 2002; Balco and Rovey, 2010; Valletta et al. 2017) and with our strong dependence on the organic carbon ^{14}C chronometer (Muller, 1977; Snyder and Bryant, 1992; Muller and Calkin, 1993).

While radiocarbon is used extensively to determine the age of post LGM glacial landforms (e.g., Muller and Calkin, 1993) the use of in-situ cosmogenic radionuclides ^{10}Be , ^{26}Al and ^{14}C (Granger et al. 2013) to determine the age of moraines, nunataks, and buried tills is on the rise (Briner et al., 2003; Balco and Rovey, 2010; Balco, 2011; Bierman et al., 2015). Using cosmogenic nuclide concentrations to argue for minimal glacial erosion under frozen based glaciers (Stroeven et al. 2002) or the duration of cover by glaciers (Bierman et al. 1999; Bierman et al., 2015) is also becoming more common. However, quantifying the amount, rate, and timing of pre-LGM glacial erosion, even with million-year half-life cosmogenic nuclide chronometers, remains challenging because of the strong depth dependence of nuclide production in the upper

meters of the surface, and the high potential for violating steady-state assumptions including erosion rate. In order to constrain integrated histories of glacial erosion, new approaches using cosmogenic nuclides must be explored.

This study determines the magnitude of glacial erosion along the northern escarpment of the Appalachian Plateau between the Finger Lakes and Mohawk Valley Regions of New York State (Fig. 1). The study area spans the sharp physiographic boundary between the smooth, relatively undissected long-wavelength topography of the Finger Lakes and the shorter wavelength fluvially dissected landscape of surrounding areas. Exploiting a stratigraphically continuous sandstone layer present throughout the study area (Fisher et al., 1970), I estimate the amount of glacial erosion experienced by the landscape over the last million years using the concentration of cosmogenic ^{10}Be , which is produced at an increasing rate as a rock layer moves towards the earth's surface (Gosse and Philips, 2001). The measured ^{10}Be concentrations, combined with the timing of the glacial periods inferred from the marine isotope curve (Lisiecki and Raymo, 2005), are used to model plausible erosion scenarios related to successive glacial periods over the last million years.

Regional Setting

Bedrock geology

Dominating the bedrock lithology of New York State are the Devonian sedimentary rocks of the northern Appalachian Basin (Oliver et al, 1967; Fisher et al., 1970). The Appalachian Basin, a foreland basin, developed adjacent to the Paleozoic orogenies which stretch from Maine to Alabama (Ryder, 1995). The Finger Lakes roughly coincide with the trough of the Devonian Appalachian Basin where sedimentary facies consist of black and dark grey shales with more competent lithologies more prevalent on the shelves to the east and west (Fig. 2B) (Gray, 1991).

The Lower Devonian Tristates group contains the quartz rich Oriskany Sandstone and overlying Onondaga Limestone, which are typically separated by less than 5 meters within the study area. The middle Devonian Hamilton and Genesee Groups that overly the Onondaga limestone are composed of interbedded shales, limestones, siltstones and sandstones that were deposited in a marine environment (Fig. 3). In New York, the Oriskany Sandstone is one of the few coarse-grained quartz sandstones exposed along the topographic escarpment of the Appalachian Basin (Oliver et al., 1967) and in nearby aggregate quarries where it occurs it is as much as 30 m below the surface. It is nearly pure quartz which makes it ideal for the cosmogenic nuclide analysis in this study and its broad regional extent and horizontal orientation make it an ideal datum for evaluating regional patterns in glacial erosion.

Pleistocene glaciations

During the Last Glacial Maximum (LGM) nearly all of New York State, apart from the Salamanca re-entrant, at the SW edge of the state, was covered by ice (Snyder and Bryant, 1992). The Salamanca re-entrant was not covered by glacial ice during any of the North American glaciations and the surrounding area preserves moraines associated with both the Illinoian and Wisconsinan glaciations (Snyder and Bryant, 1992). In addition to the Wisconsin and Illinoian moraines preserved around Salamanca, a pre-Illinoian moraine is present in NE Pennsylvania (Fullerton, 1986). These moraines are evidence that the Laurentide ice sheet advanced to cover New York State a minimum of three times during the last million years (Fig. 1).

One of the most prominent glacial landscapes of New York State is the Finger Lakes Region (FLR), composed of eleven elongate troughs, some containing lakes, that splay out from the north towards the south; the deepest of which is Cayuga Lake whose lake floor is 140 m below sea level (von Engeln, 1961; Mullins et al., 1996). The Valley Heads Moraine coincides

with the southern ends of the Finger Lakes troughs (Fig. 1), and it also coincides with a major physiographic transition from a long-wavelength high relief topography north of the moraine to a short-wavelength, fluvially dissected topography to the south. The southward fanning form of today's Finger Lakes led early researchers to suggest that the lakes were likely part of an ancient river network which drained northward prior to being excavated by glacial erosion into the mechanically weaker facies of the Devonian bedrock (Brigham, 1893; Tarr, 1893; von Engeln, 1961; Mullins et al., 1996; Bloom, 2004). Tarr (1893) attributed the majority of landscape modification into these weaker rocks to the initial glacial episode, which implies that the physiographic change north and south of the Valley Heads Moraine is a long-standing feature, despite multiple glaciations. In order to explore this hypothesis, it is necessary to look beyond the most recent glaciation, which overprints or outright removes the surficial glacial formations/deposits of previous advances.

While there are burial ages on tills in central Missouri as old as 2.58 Ma (Balco and Rovey, 2010), we focus on the last million years when global ice volume was similar to the Laurentide ice sheet at the LGM. Ice sheet modeling of the last 400,000 years shows the correlation between the eccentricity cycle (100ka period), which dominated the last million years, and high $\delta^{18}\text{O}$ values. Global ice volumes are inferred from the marine isotope curves derived from benthic $\delta^{18}\text{O}$ records (Lisiecki and Raymo, 2005). We assume that it is only during periods where the $\delta^{18}\text{O}$ values and thus global ice volumes are similar to that of the LGM that the ice sheet extended far enough south to reach the study area (Lisiecki and Raymo, 2005). Using this approach, we identify a total of five glacial periods (marine isotope stages (MIS) 2, 6, 10, 12, and 16) where ice most likely covered our study area and extended further south. A northern hemisphere ice sheet model (IcIES) coupled with a general circulation model spanning the last

400 ka suggests glacial advances over the study area during MIS 2 and 6 (Abe-Ouchi et al., 2013).

Cosmogenic Nuclides

Cosmogenic nuclides are produced through two major pathways; primary and secondary cosmic rays. Primary cosmic rays, high energy particles (the majority of which are protons) originating from outside our galaxy, interact with the atmosphere and the upper most portion of the earth's surface (Friedlander, 1989). The collision of protons with atoms in the atmosphere produces secondary cosmic rays and ultimately results in a cascade of secondary particles that interact with atoms in the earth's atmosphere and crust to result in the production of cosmogenic nuclides (Friedlander, 1989; Dunai and Lifton, 2014).

In quartz, the collision between the cosmic-ray derived high energy particles and atoms of silica and oxygen results in the in-situ production of radionuclides ^{26}Al and ^{10}Be , with half-lives of 700 ka (Norris et. al., 1983) and 1.38 Ma (Chmeleff et al., 2010; Korschinek et al., 2010), respectively. Nearly all ^{26}Al and ^{10}Be in near-surface rocks are produced by cosmic ray interactions (Sharma and Middleton, 1989). The concentration of a given in-situ cosmogenic radionuclide, specifically in quartz, is controlled by the production rate, which varies according to variations in the cosmic ray flux, the erosion rate, and the depth and elevation dependencies related to each production mechanism, as well as the decay rate (Lal, 1991; Phillips et al., 2016).

Spallation is the dominant cosmogenic nuclide production mechanism in the upper three meters of regolith and rock, and results from the collision of high energy nucleons that remove protons and neutrons from the atomic nuclei resulting in lighter nuclei (Dunai and Lifton, 2014). The surface spallation production rate of ^{10}Be at sea level and high latitude is 4.09 ± 0.39 atoms $\text{g}^{-1} \text{yr}^{-1}$ (Lifton et al, 2014; Phillips et al. 2016). Below three meters, production is dominated by

muons, which interact more weakly with matter, resulting in greater penetration depths (Dunai, 2010).

Muons are negatively charged particles resulting from the decay of pions created in the upper atmosphere through the interaction of primary cosmic rays and atomic nuclei (Dunai, 2010). There are two main types of muon reactions; slow and fast muons. Slow muons are the result of negative muon capture that occurs when an atom's electron cloud captures a slowed/stopped muon, which ultimately neutralizes a proton in that atom's nucleus (Dunai and Lifton, 2014). Fast muons create secondary neutrons, and ultimately cosmogenic nuclides, through breaking radiation (*Bremstrahlung*) of sufficiently high energy (Dunai and Lifton, 2014). At the Earth's surface at sea level the slow muon production rate for ^{10}Be is $0.012 \text{ atoms g}^{-1} \text{ yr}^{-1}$ and the fast muon production rate for ^{10}Be is $0.039 \text{ atoms g}^{-1} \text{ yr}^{-1}$ (Braucher et al., 2011).

This study focuses on the use of in-situ ^{10}Be measured in samples collected more than 8 meters below the current ground surface; thus, we only consider production by slow and fast muons. Samples of the Oriskany Sandstone at depth allow for comparison across the study area, with differing cosmogenic nuclide concentrations reflecting variable exposure histories and the different amounts of erosion that occurred above the Oriskany Sandstone (Fig. 4). Forward models of alternating ice shielding and glacial erosion events are used to determine a range of plausible time-erosion events that match measured concentrations. The concentration of the cosmogenic nuclide ^{10}Be in the sample is the ultimate output of the model (see below).

Methods

Sampling

The Oriskany Sandstone was sampled at varying depths in the landscape along the northern escarpment of the Appalachian Plateau along a roughly E-W transect during the fall of 2016 (Fig. 2A). Sampling sites were dictated by the access to the quarries and road cuts that exposed the Oriskany Sandstone. At each sampling locality we determined the depth below the surface based on information provided by the quarry operators or by making measurements in the field with a laser range finder.

Surface reconstruction

Accurate determination of the Oriskany Sandstone's depth below the surface at each site is essential in order to accurately interpret and model cosmogenic nuclide concentrations in the context of glacial histories. We used historic USGS topographic maps, with vertical resolutions ranging from six – three meters, in conjunction with the measured elevation of the Oriskany Sandstone in each quarry to determine the depth of the Oriskany Sandstone layer below the original surface at this specific site. For example, at the Oriskany Falls Quarry (Fig. 2A), the top of the Oriskany Sandstone has an elevation of 341.4 m.a.s.l and the pre-quarry surface elevation is 371.9 m.a.s.l., which yields a depth of 30.5 meters below the surface (Table 1).

Sample processing

A total of six samples from 5 localities were processed at Syracuse University to isolate pure quartz. Samples were crushed and milled and sieved to a grain size of 250 to 750 microns. Subsequently, samples were treated with aqua regia to remove carbonate and grain coatings, etched on heated rollers at 40°C in a solution of 5% nitric acid and 5% hydrofluoric acid prior to etching in a 1% hydrofluoric and 1% nitric acid solution within an ultrasonic bath. Post etching, 250 mg of sample were dissolved in 5 ml of concentrated HF with 1% H₂SO₄ and fumed. The residual H₂SO₄ was diluted with pure H₂O to assess quartz purity by measuring the

concentrations of Be, Fe, Ca, Al, Ti, Na, K by Inductively Coupled Plasma Optical Emission Spectrometry (ICP-OES) at SUNY-ESF. At the University of Vermont, 20 g of purified quartz from each sample was dissolved and ^{10}Be was isolated by cation exchange chemistry before being converted to BeO, mixed with Nb and packed for Accelerator Mass Spectrometry (AMS) analysis (Corbett et al., 2016) at Purdue University's PRIME Lab.

Modeling glacial erosion

We employ a forward numerical model to explore the range of the glacial erosion histories consistent with the measured concentrations at each sampling site and assume that only the last 1 Ma of Earth history, dominated by the eccentricity orbital forcing (Abe-Ouchi et al., 2013), results in glacial episodes affecting the Finger Lakes and Mohawk Valley regions. Lisiecki and Raymo's (2005) global benthic δO^{18} record is used to determine periods during which the Finger Lakes Region (FLR) when: 1) glacial ice would shield in-situ cosmogenic nuclide production, 2) in-situ production during ice free periods and 3) to specify when glacial erosion events transported the Oriskany Sandstone towards surface subjecting it to a change in production rate. A graphical representation of the effects depth, production mechanism, and shielding have on concentration are shown in Figure 4. The concentration through time is determined using the following equation, slightly modified from Lal (1991) to account for shielding by glacial ice:

$$N(x, t) = N(x, 0)e^{-\lambda t} + I(t) \frac{P_0}{(\lambda + \mu\epsilon)} e^{-\mu x} (1 - e^{-(\lambda + \mu\epsilon)t})$$

where N = concentration; x = depth; t = time; λ = decay constant; P = production rate; ϵ = erosion rate and I = ice cover. (Table 2)

Ice cover, I , is treated as a binary that invokes complete shielding during inferred times of cover by glacial ice. Periods of ice cover are determined by a threshold $\delta^{18}\text{O}$ values $> 4.3\text{‰}$ on a smoothed (5 ka moving window) version of the marine isotope stack (Lisiecki and Raymo, 2005) to remove high frequency variations; otherwise we consider the landscape to be subject to standard surface production rates. Carbon dating of debris at the South Dansville site, located in Central New York, west of the FLR, yields ages between 14 ka and 15 ka for the Valley Heads Moraine (VHM) which corresponds to an approximate $\delta^{18}\text{O}$ value of 4.3‰ (Muller and Calkin, 1993) (Fig. 1). This threshold, however, results in an unrealistic number of potential glacial events compared to the number observable in the models; therefore, we focused on the largest positive MIS excursions 2, 6, 10, 12 and 16 as the most likely to generate similar southern ice extents. This choice is supported by the three preserved terminal moraines of Wisconsinan (MIS 2), Illinoian (MIS 6), and Pre-Illinoian (MIS 10) age in NY and in northern PA (Fullerton, 1986). The duration of ice cover is assumed to be a relatively brief period of time (≤ 30 ka) based on numerical models of the LGM (Abe-Ouchi et al., 2013) and the rate of ice recession since the LGM (e.g. Muller and Calkin 1993). Under this scenario, cosmogenic nuclide concentrations would be most impacted by shielding, while the effect of decay is negligible over the duration of a shielding event.

Random variations in the magnitude of glacial erosion, which results in the movement of the Oriskany Sandstone toward the Earth's surface, are invoked during the switches from ice cover to ice free conditions according to a random draw from a gamma distribution. More specifically, a matrix of varying erosional magnitudes (changes in depth) is created using the gamma distribution which is modified through the manipulation of its shape and scale factors (Table 2). This allows for the tailoring of the matrix to the magnitude of erosion inferred from

the depth of the OS at each site. The rationale behind this choice is that production resumes after the glacier recedes regardless of when erosion occurred during advance, ice cover or recessional phase of glaciation. A total of 10,000 simulations of erosion related to the timing of Marine Isotope Stages 2, 6, 10, 12 and 16 are generated and are used to forward model cosmogenic nuclide concentrations. Erosion pathways are randomly generated from a gamma distribution for each MIS event we consider and summed to determine the total erosion. Random erosion pathways are generated to create 10,000 simulated erosion histories between the sample collection depth and the bottom of the production window, defined as where production is < 1% surface fast muons production rates. The starting depth of each erosion history is assumed to have a starting concentration that reflects secular equilibrium at a background erosion rate of 25 m Myr⁻¹ (Matmon et al., 2003a; Matmon et al., 2003b; Reuter et al., 2003). The subset of model solutions within the two-sigma uncertainty of the measured cosmogenic nuclide concentrations reflect plausible scenarios for glacial erosion histories that best explain the observed concentrations.

Results

Cosmogenic nuclide concentrations

The AMS measurements and the ¹⁰Be concentrations for the six samples are listed in Table 1. The concentration of ¹⁰Be ranged from 4,600 atoms g⁻¹ to 2,700 atoms g⁻¹ and two of the samples were below detection limit. Uncertainties are high because the low concentrations of ¹⁰Be and the small aliquots of quartz dissolved resulted in concentrations near the instrumental detection limit. Reanalysis of larger aliquots of quartz for the no-detect samples are in progress. ¹⁰Be concentrations yield apparent ages between 17.5 ka to ~ 300 ka and erosion rates vary between 637 m Myr⁻¹ and 43 m Myr⁻¹ for depths ranging from 10 m to 30 m and production rates

between 0.0108 atoms g^{-1} and 0.0303 atoms g^{-1} . From west to east the calculated age at each site varies a great deal with no real consistent trend based solely on changes in longitude (Fig. 7). The lowest erosion rates are on the same order of magnitude as the Appalachian background erosion rates of 25 m Myr^{-1} (Matmon et al. 2003a; Matmon et al. 2003b; Reuter et al., 2003) (Fig.7).

Mean erosion rates and effective ages

Mean erosion rates and effective ages were calculated for each site, including the sites below detection limits (Table 1). Ages and erosion rates are calculated assuming constant depth and constant erosion rate (Lal, 1991), which is unlikely at 4 of the 5 sites, thus it is important to remember that these values only serve to determine whether the erosion was LGM or earlier in timing and whether it significantly differed from the background erosion rate.

Glacial erosion modeling

The 10,000 erosion pathways explore the extremes of erosion scenarios from background continental erosion to large magnitude erosion during the LGM (Fig. 5b). The subset of model runs that reflect the measured concentration narrows the number of possible erosion scenarios (Fig. 5a) and are used to calculate median, mean and the 1-sigma envelope about the mean for each model time step (Fig. 5). At the sites with no measurable ^{10}Be , we assumed a concentration of >1000 atoms g^{-1} as an initial exploration of the erosion history at both no-detect sites. The size of the erosion events ranged from extremes up to 60 m to small events indistinguishable from our prescribed background erosion rate of 25 m Myr^{-1} . Our forward modelling shows that the largest events occurred as a consequence of the LGM (MIS 2) or at the penultimate glaciation (MIS 6).

Discussion

Early work in the Finger Lakes attributed the majority of erosion to the first advance of the glacier and promoted variations in the competence of the Devonian substrate as the ultimate control on the total amount of erosion (Tarr, 1902; von Engel, 1961). Assumptions on the timing of glacial erosion, consistency of that timing and the reasons beyond the variation need to be further explored. Our results generally indicate that pre-glacial topography had an effect on the magnitude of erosion; for example, the highest topographic positions in the landscape east of the Valley Heads Moraine experienced minimal glacial erosion. In terms of the timing of the glacial erosion, our results suggest more recent erosion during the Wisconsinan and Illinoian glaciations clearly impacted areas both north and south of the Valley Heads Moraine with variations in the magnitude and timing of erosion linked to differences in elevation.

Data interpretation

Seneca Stone and Han1601: Insights from unmeasurable concentrations

The Seneca Stone Quarry (Seneca Stone) is the westernmost site in the transect with a reconstructed surface elevation of ~170 meters and the Oriskany Sandstone formation located approximately 9 meters below the surface. The erosion rate and effective age, calculated using the assumed concentration of 1000 atoms g^{-1} at a depth of 9 m with a production rate of 0.0303 atoms g^{-1} (Table 1) for this site, were extremes in the transect in that this site experienced the highest calculated erosion, 640 m Myr^{-1} , and had the youngest calculated effective age, 30 ka. This magnitude of erosion would have had the potential to obliterate the pre-glacial fluvial dissected landscape which is still visible in adjacent areas. Examination of the local topography reveals that elevations are relatively flat (within 50 meters) to the immediate north and south of this site (Fig. 8a). In terms of the timing of the glacial events, the calculated age indicates that the

majority of erosion and exhumation would be coincident with the Last Glacial Maximum (MIS 2). Our modeling indicates ~ 60 m of erosion at MIS 2; a value determined by measuring the size of the “step” (the change in depth) in the median simulation at MIS 2 (Fig. 6). Located in the trough of the Appalachian Basin, where lithologies are the weakest, a high amount of glacial erosion does not seem unreasonable. Furthermore, this modeled magnitude of erosion is within the range of estimated global quaternary glacial erosion rates which are between $0.00001 \text{ cm yr}^{-1}$ and 1.0 cm yr^{-1} (Delmas, 2009). Our modeling implies that the broad ridge separating Seneca and Cayuga Lakes was ~ 60 m higher prior to the last glacial advance (Fig. 6). If each of the four previous glaciations were responsible for similar amount of erosion, which is unresolvable in our model due to the high magnitude of last glacial erosion, the elevation of the original inter-lake land surface would be similar to that observed at the uplands at the southern end of the Lakes and the landscape south of the Valley Heads Moraine.

At Jamesville (Han1601), our assumed concentration of $1000 \text{ atoms g}^{-1}$ in conjunction with a depth of 18 m and a production rate of $0.0193 \text{ atoms g}^{-1}$ (Table 1) yields erosion rates and apparent ages of 440 m Myr^{-1} , and 45.0 ka, respectively. The difference in rates between the Jamesville and Seneca Quarries sites reflects the difference in the depth of the Oriskany Sandstone below the surface. Nonetheless, the calculated age and the mean simulation in the model output of 50 meters indicate that the majority of erosion occurred during MIS 2. The upper surface of the Jamesville Quarry is at ~240 m.a.s.l, approximately 60 m above Seneca Stone. The topography in and around the site is complex, more specifically the quarry is bounded by melt water channels and a small field of drumlins to the north. The drumlins are the product of the last glacial period, however the age of the bedrock melt water channels, while dated by radiocarbon on sediments, is not known directly (Kehew et al., 2009). Topographic profiles

indicate that the Jamesville Quarry lies at the base of a steep ramp (7% grade) up onto the Appalachian Plateau (Fig. 8c). Given the proximity to the Tully and Jamesville Glacial troughs, ice flow around high points in the topography could have resulted in locally enhanced erosion. Alternatively, the creation of surrounding valleys is attributed to the drainage of proglacial lakes during the retreat of the Laurentide ice sheet (von Engel, 1961). Erosion at the Jamesville Quarry may have been augmented erosion related to glacial lake water draining from W to E through this area.

Han1602

Located between the two no-detect sites, the sample from the Skaneateles Quarry (Han1602) has a surface of elevation of 250 meters with the Oriskany Sandstone formation located 25 meters below the surface. The erosion rate of 110 m Myr^{-1} was calculated at a depth of 25 meters with a production rate of $0.0141 \text{ atoms g}^{-1}$ (Table 1) and is less than a quarter of the erosion rates modeled at the Jamesville and Seneca Quarries. Similar to the Jamesville Quarry area, this area also hosts bedrock channels related to the floods that drained the integrated glacial Lake Watkins. In contrast to the very low concentration sites, this quarry lies at the upper edge of a topographic ramp (Fig. 8b). The median model simulation predicts $\sim 30 \text{ m}$ of erosion occurred at MIS 6, the penultimate glaciation. The calculated age for this site is 180 ka, which also correlates well with MIS 6.

Han1603 and Han1604

Han1603 and Han1604 are two samples collected from the Oriskany Falls Quarry located at the easternmost edge of the FLR, specifically the area bordered by the Valley Heads Moraine. This site is located at the highest elevation in the transect, 370 m, with the Oriskany Sandstone formation located at a depth of 340 m. The ages of the two samples were calculated to be 380 ka

and 390 ka respectively, while the calculated erosion rates are 44 m Myr⁻¹ and 43 m Myr⁻¹. These values were calculated using a depth of 30 m and a production rate of 0.0108 with the variation in the ages stemming from differences in the measured ¹⁰Be concentrations (Table 1). The erosion rates calculated from these samples as well as the median model output, which has minimal changes in depth at each of the marine isotope stages, indicate that this site experienced minimal erosion, the closest to the background erosion 25 m Myr⁻¹ which we prescribed in modeling the erosion histories at each site. The magnitude of the steps in the model output for both samples indicate that this site eroded at a rate that was indistinguishable from the prescribed background erosion rate. The area in and around the Oriskany Falls Quarry has been clearly modified by focused erosion concentrated in preexisting fluvial valleys, however, Oriskany Falls sits on a broad bench behind the main topographic escarpment of the Appalachian Plateau (Fig. 8d). The position south of the topographic escarpment must have limited the ability of glaciers to do significant work on the landscape.

I88S

The easternmost site in the transect and the only site located outside the Finger Lakes Region, I88S is in the rough fluvially dissected terrain of the surrounding areas. The I88S site is located south of a drumlin field at an elevation of 287 meters with a reconstructed surface elevation of ~300 meters and has a calculated erosion of 120 m Myr⁻¹, and an effective age of 140.0 ka. A production rate of 0.0259 atoms g⁻¹ and a depth of 12 m were used to make these calculations (Table 1). The mean simulation of the model output indicates that this site experienced the vast majority of erosion, ~30 meters, during the penultimate glaciation (MIS 6). Further examination of the local topography reveals that this site is just south of a relatively flat area (excluding the drumlins) and north of an area of rugged/rough high elevation terrain that is

bounded by large river valleys to the North and East (Fig. 8e). The drumlins north of the site indicate that the ice flowed to the SW, while the contrasts in the local topography indicates that the erosion was focused in the valleys.

Overall it appears that within the heavily glaciated Finger Lakes Region, the westernmost and lowest elevation sites experienced the highest rates of erosion, with calculated values more than triple that of the background erosion rate. The swath profile of the Seneca Stone site highlights the relatively flat terrain, more specifically there is little difference between the maximum and minimum elevations across this profile, and low (>200 m) topography characteristic of the northern and western portions of the FLR (Fig. 8a). On the other end of the transect at the eastern limits of the FLR the site located at the highest elevation experienced the least erosion, with effective erosion rates that are less than double the background erosion rate and with the modeled erosion rates being well within background. The swath profile of the Oriskany Falls site highlights an area with overall higher elevations with steep changes in elevation visible to the north and south (Fig. 8d). Comparing the FLR to the adjacent regions it appears that at relatively similar elevations the timing, as determined by the model, and magnitude of erosion calculated from the ^{10}Be concentration, were analogous despite differences in topography. Comparing the Skaneateles and I88 Roadcut swath profiles, the similarities in elevation, the lack of variation between max and min, and the relatively gradual changes in elevation are apparent (Fig. 8). This indicates that the physiographic difference across these regions may owe their origins to lithological differences.

Limitations of modeling

Our modeling study of erosion rates provides insight to the variability in the glacial erosion history along the northern escarpment of the Appalachian Basin; but, it has limitations.

Muons present trade-offs in that their long attenuation length results in measurable concentrations at depth over million-year timescales. However, their attenuation length makes them less sensitive to small changes in depth. Depth profiles spaced at roughly five-meter intervals would result in a greater ability to resolve more unique erosion histories; however, the Oriskany Sandstone is the only sandstone coarse grained enough, in terms of what is necessary for cosmogenic nuclide analysis on quartz grains, across the entire study area. The ^{10}Be data could be augmented with ^{36}Cl depth profiles through the Onondaga and other limestones preserved at each site (Dunai, 2010). At a minimum, the measurement of ^{26}Al would provide an independent verification of the model results. While the relatively rapid episodes of ice cover are insignificant in terms of muon production versus the duration of shielding, our use of the MIS curves pre-supposes that the largest positive excursions are most sensitive to ice volume changes in the Laurentide ice sheet. Existing geochronology of pre-Last Glacial Maximum aged moraines in the Northeastern USA is inadequate to suppose that smaller, in terms of δO^{18} value, even numbered MIS excursions could have resulted in glaciers that covered the study area.

Conclusion

The Finger Lakes Region of Central New York represents a unique region as it is an area of smooth topography surrounded by rough topography and yet nearly the whole of New York was subject to the same erosive events, the glacial advances and retreats of the Pleistocene. Traditional thought agreed that the differences in erosion and topography could be attributed to lithological differences and that the first advance of the glacier was the one that did the vast majority of the landscape transforming work with subsequent advances finding a prepared path to traverse and thus having minimal impact on the landscape. Exploring the veracity of that statement and determining the magnitude and timing of the glacial erosion is complicated by the

nature of glacial advances and retreats and the obliteration of any surficial deposits left by previous glacial events. Cosmogenic nuclides, specifically ^{10}Be , in conjunction with the Oriskany sandstone, a flat-lying regionally extensive formation, enable this study to look beyond the most recent glaciation, the LGM, and make determinations about the previous glaciations. The ^{10}Be concentrations, ages and erosion rates varied but several patterns emerged. More specifically samples at high elevations had the oldest ages, and erosion rates similar to the background erosion rate and low elevation samples had the youngest ages and the erosion rates more than triple the background erosion rates. Comparing the Finger Lakes Region to that of an adjacent area it appears that the Finger Lakes Region experienced much more erosion.

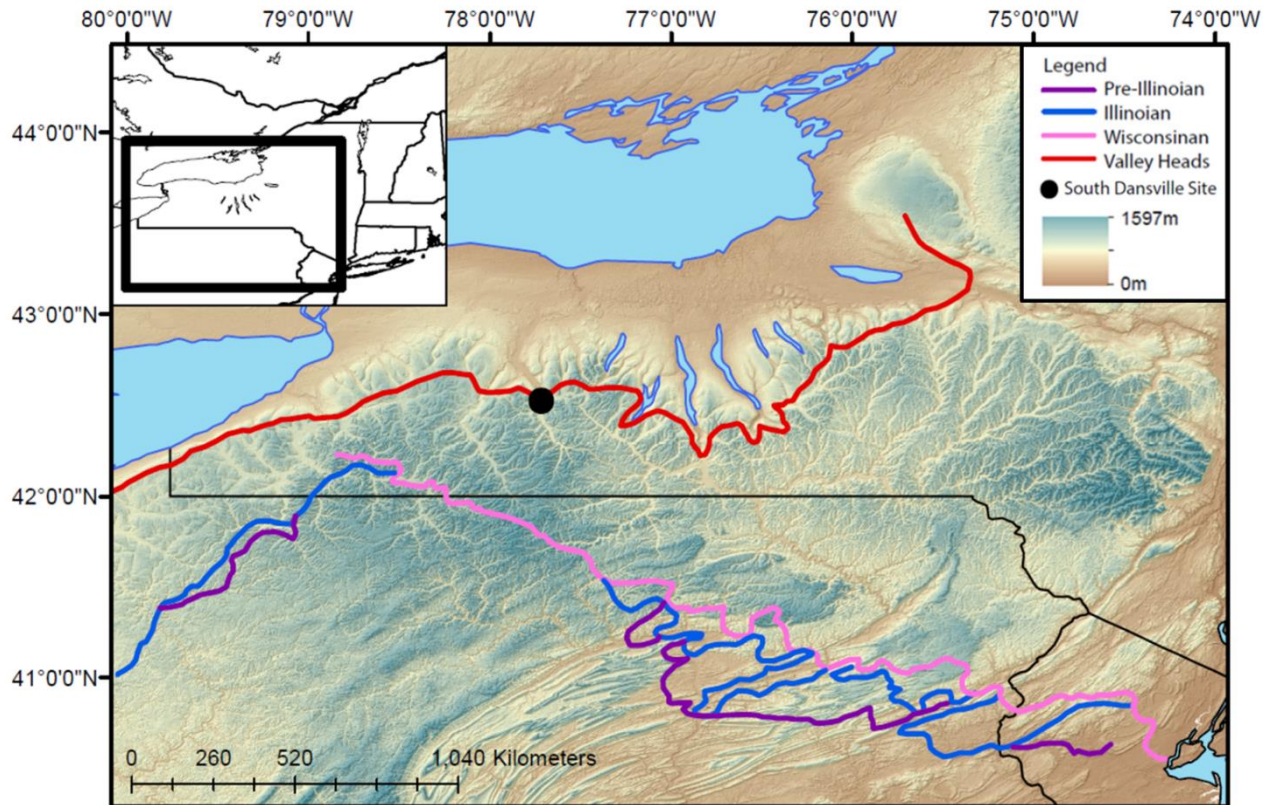
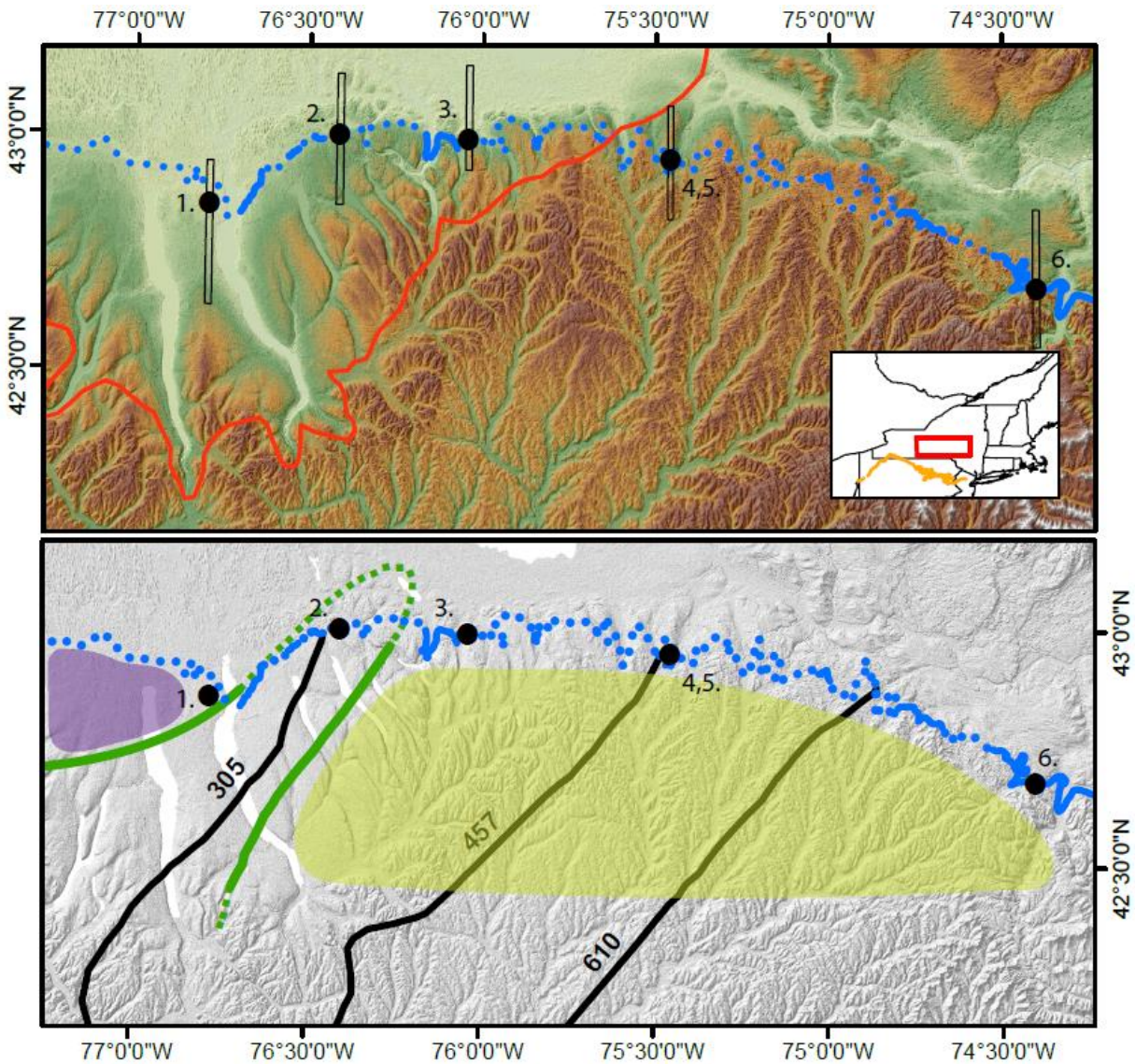


Figure 1. Regional Topographic Overview: There are three terminal moraines preserved in Southern NY and Northern Pennsylvania providing local evidence for multiple for glaciations across New York. These moraines range in age from: Wisconsinan glaciation corresponding to the LGM, ~20Ka, Illinoian glaciation, ranging from 130ka-190ka Pre-Illinoian glaciation, >200ka (Fullerton, 1986). In addition, the Valley Heads Moraine marks a physiographic transition between the smooth long-wavelength areas to the north and the rough short-wavelength areas to the south. Radiocarbon dating has been done on samples from the Valley Heads Moraine providing ages between 14 ka and 15 ka at the South Dansville Site (Muller and Calkin, 1993). Inset: Regional Area outlined in black



Legend

- | | |
|------------------------|-----------------------------------|
| ● Sampling Sites | Sampling Site Locations |
| ⋯ Oriskany Sandstone | 1. Seneca Stone Corporation |
| — Valley Heads Moraine | 2. Hanson Skaneateles Quarry |
| — Terminal Moraine | 3. Hanson Jamesville Quarry |
| ■ Eastern Shelf | 4,5. Hanson Oriskany Falls Quarry |
| ■ Western Shelf | 6. I88 Road Cut |
| ⋯ Trough Margin | Swath Profile |
| — Isopach Lines (m) | (see Figure 7) |

Figure 2: A) Digital Elevation Model (SRTM) showing the topography of the landscape. B) Isopach Map of Middle Devonian Facies. (Oliver et al., 1967) and Paleogeographic reconstruction of New York State during the Middle Devonian. (Gray, 1991; Fisher et al., 1970).

Inset: Study area location outlined in red

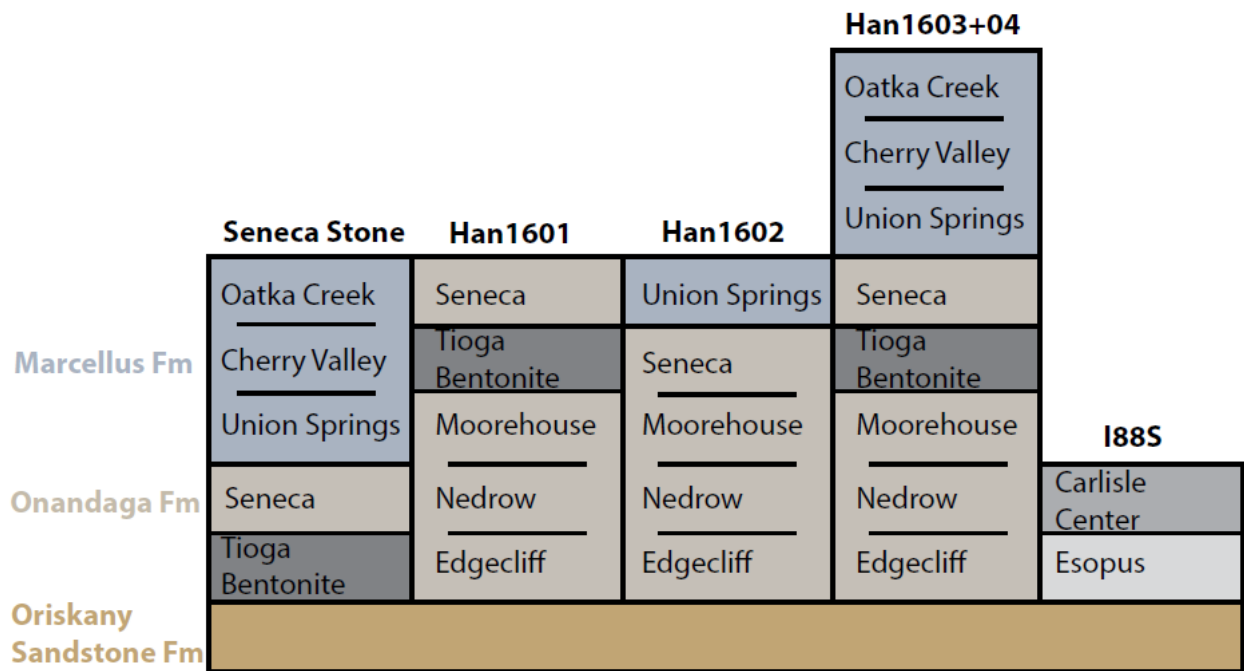


Figure 3. Stratigraphic Column: The formations overlying the Oriskany Sandstone Formation at each of the sampling sites (Rogers et. al., 1990; Anderson and Goodwin, 1991; Selleck, 2010; Additional Materials Provided by Quarry Operators).

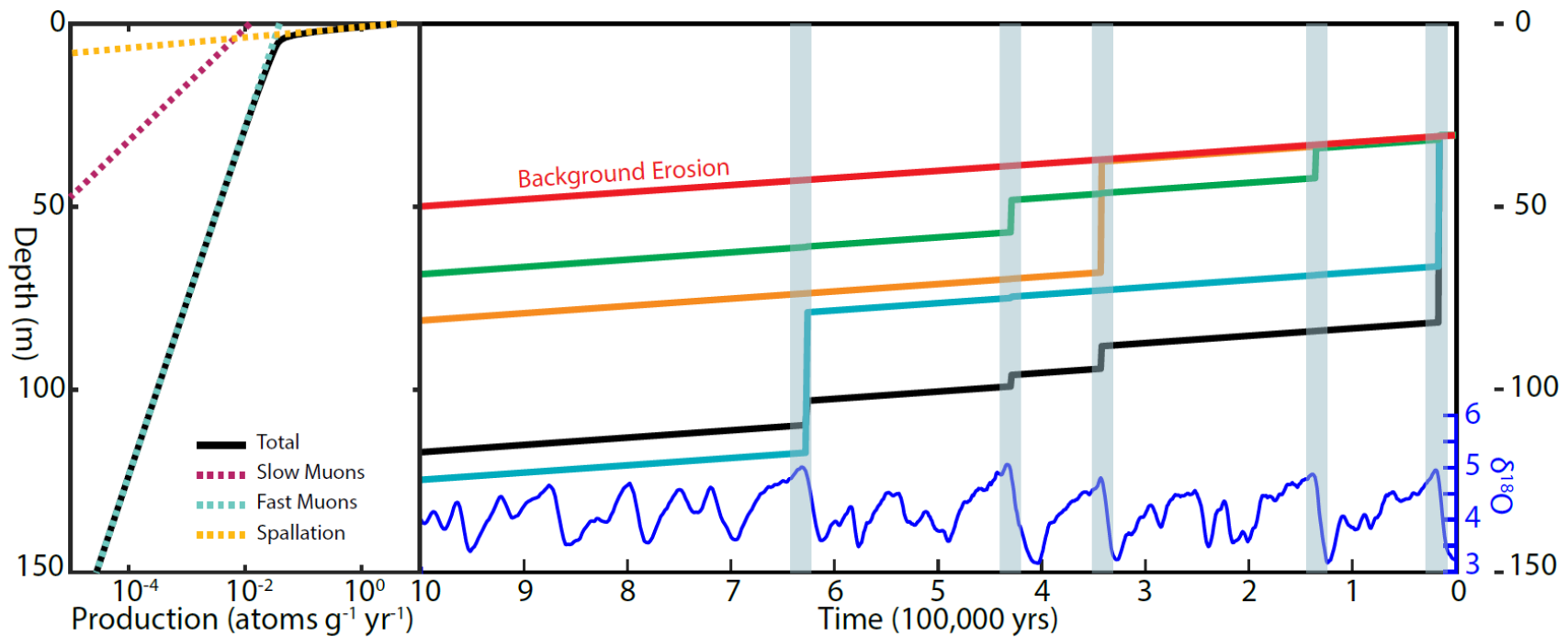


Figure 4. Conceptual Model Diagram: The interaction between the Oriskany Sandstone, periodic glacial events derived from the Lisiecki and Raymo (2009) Marine Isotope Curve (blue plot at the bottom of the graph), depth, time, and varying cosmogenic nuclide production mechanisms. As time increases each successive glacial event has the potential to result in some quantity of erosion; exhuming the target layer toward its depth at the time of sample collection and changing the amount/type of cosmogenic nuclide production in a stepwise fashion. Each of the lines on the graph represents a different erosive scenario with the target layering starting at various depths. Red: only the proscribed background erosion rate (25 m Myr⁻¹) effects the depth of the target layer. Green: MIS 6 and 12 had large erosion events. Orange: MIS 10 had a large erosive event. Teal: MIS 16 and 2 had large erosion events. Black: MIS 2 had a large erosion event.

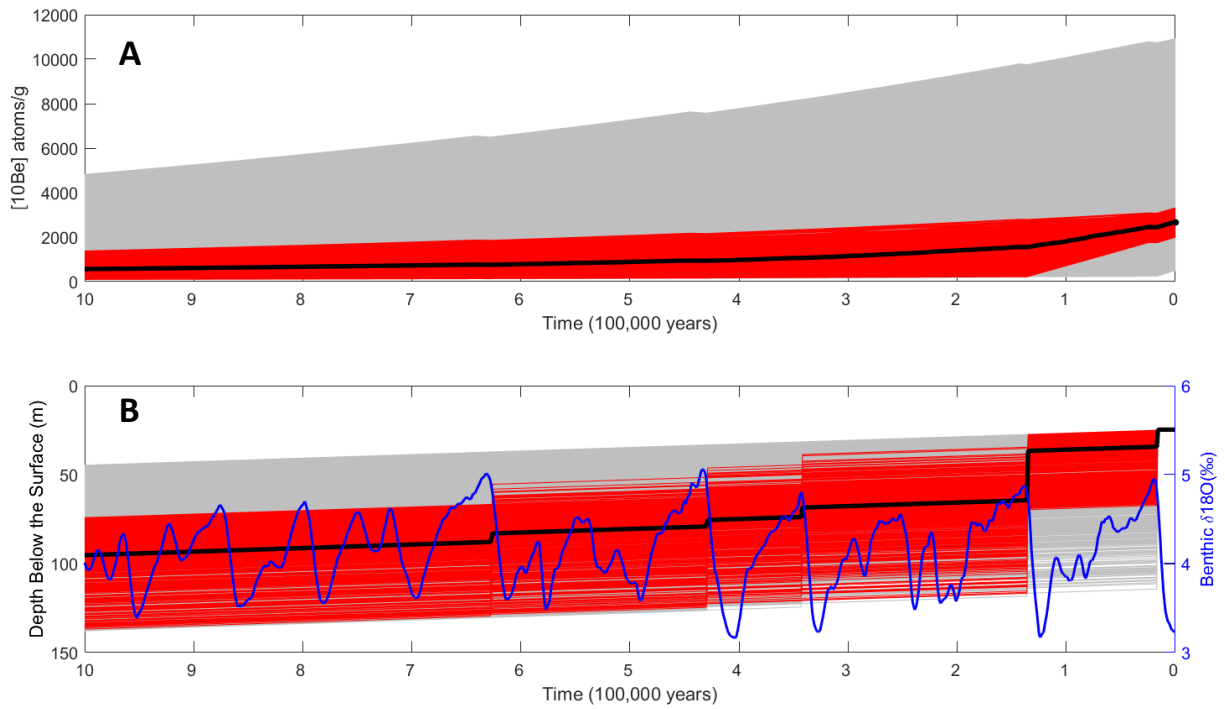


Figure 5. Simulations at Han1602: In grey are all 10,000 simulations. The red simulations are the within one standard deviation of the observed value. A) Simulated ^{10}Be concentration through time compared to the observed concentration, indicated by the black arrow. The bold black line indicates the median path/simulation. B) Change in depth over time, ultimately resulting in the modern target layer depth of ~25 meters. The bold black line indicates the median path/simulation. The Lisiecki and Raymo (2005) Marine Isotope Curve is in blue.

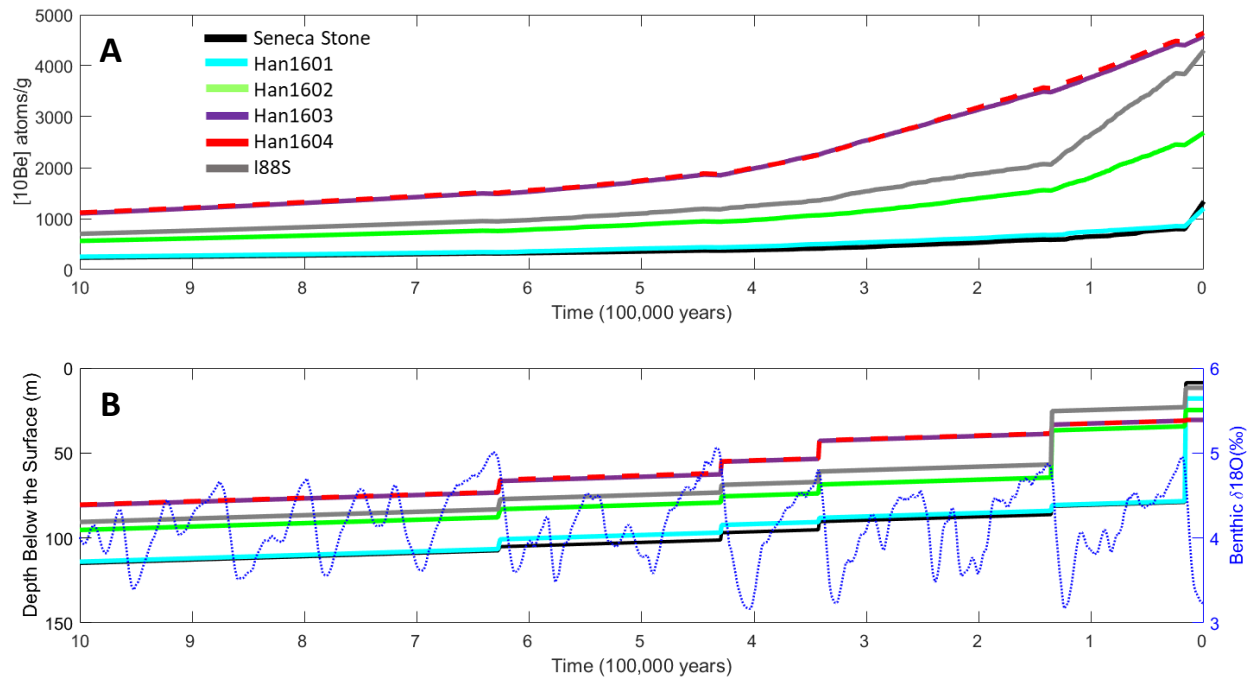


Figure 6. Model Output Summary Figure: A) Median Path/Simulation with respect to concentration vs. time for each of the 6 samples. Changes in the slope of the lines represents changes in production rate resulting from changes in depth. B) Median Path/Simulation with respect to depth vs. time for each of the 6 samples. Steps in each of the lines represents changes in depth resulting from corresponding glacial/erosive events (Blue dotted line: Lisiecki and Raymo Marine Isotope Curve (2005)).

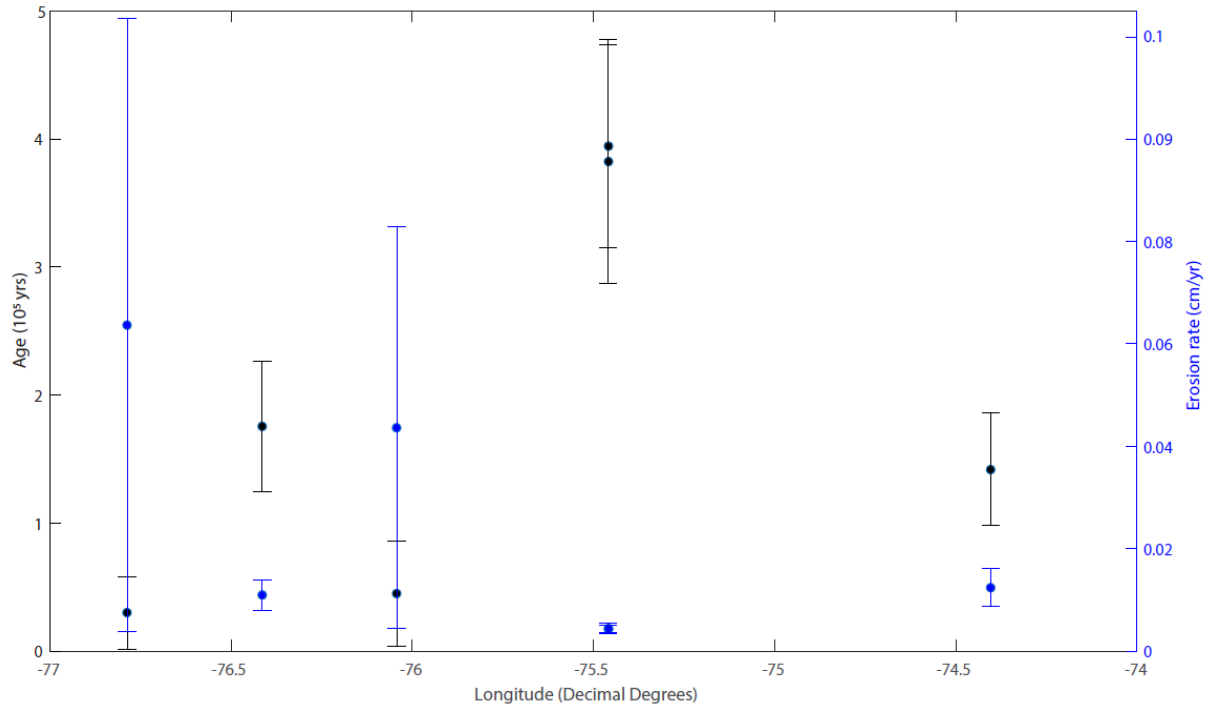


Figure 7. Plot of calculated ages and erosion rates vs. longitude, allowing for comparison of these values from west – east.

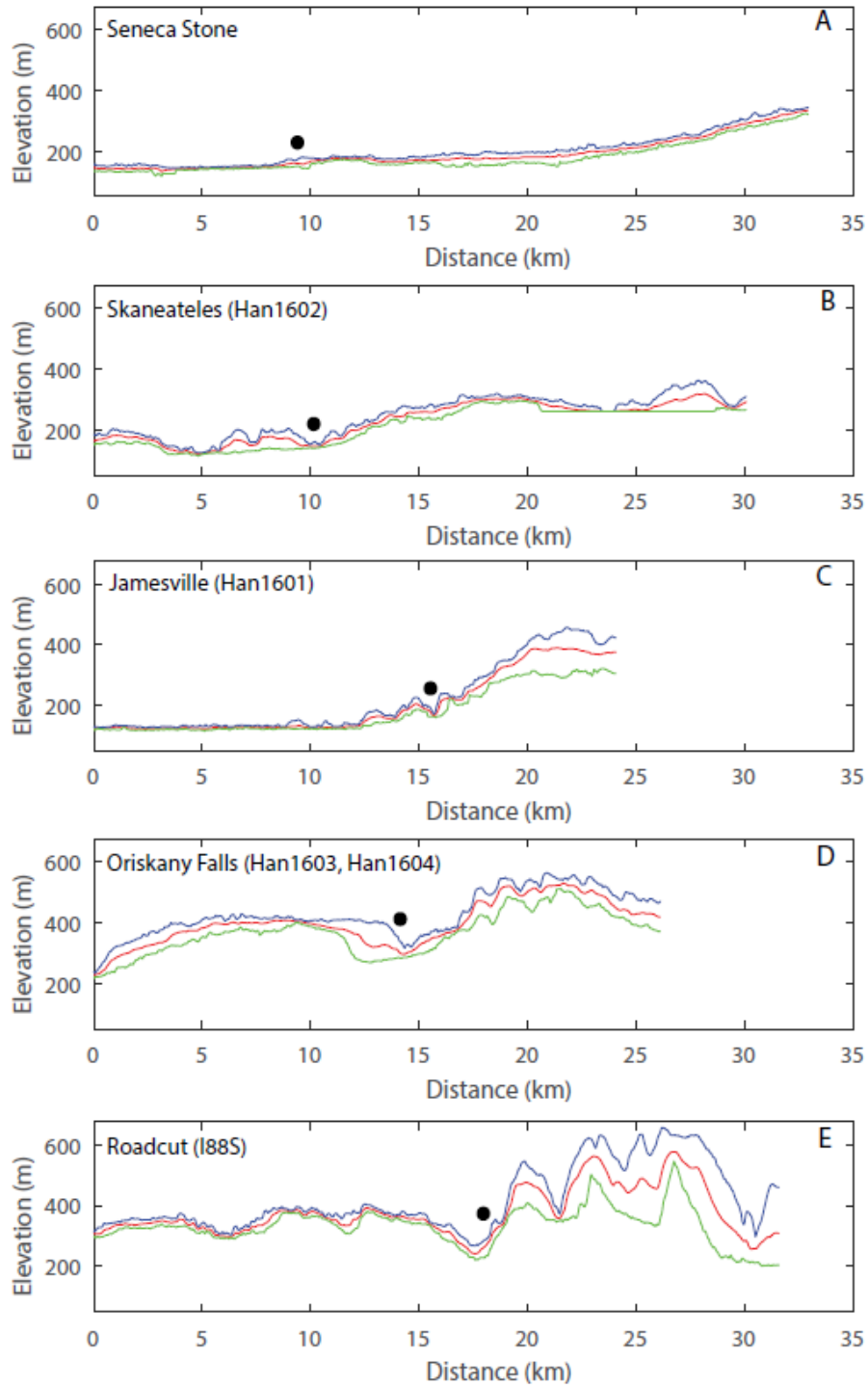


Figure 8. Sampling Site Swath Profiles: North to South profiles with a width of 2 km for each of the profiles while length varies from 18-30km. The black dots on each of the profiles represents the approximate location of each of the sites within the profile. Blue: Maximum elevations. Red: Average elevations. Green: Minimum elevations.

Table 1: Sample Data: The names of the two no-detect sites are in red.

Sample ID	Sample location	Lat.	Long.	[¹⁰ Be] (atm g ⁻¹)	[¹⁰ Be] Unc. (atm g ⁻¹)	Surface elevation (m)	Elevation of Oriskany sandstone (m)	Depth to sample (m)	Production at depth (atm g ⁻¹)	Erosion rate (cm yr ⁻¹)	Erosion Rate unc. (cm yr ⁻¹)	Age (ka)	Age unc. (ka)
Seneca Stone	Seneca Stone Quarry	42.85472	-76.78694	No Detect	938	168	160	9	0.0303	0.064	0.0599	30	28
Han1601	Jamesville Quarry	42.99472	-76.04306	No Detect	894	238	220	18	0.0193	0.044	0.0392	45	41
Han1602	Skaneateles Quarry	43.00194	-76.41417	2600	662	250	225	25	0.0141	0.011	0.00294	180	51
Han1603	Oriskany Falls Quarry	42.95528	-75.45944	4500	952	372	341	30	0.0108	0.0044	0.00106	380	96
Han1604	Oriskany Falls Quarry	42.95528	-75.45944	4600	661	372	341	30	0.0108	0.0043	0.000774	390	79
I88S	I88 Roadcut	42.68	-74.40444	4100	1148	299	287	12	0.0259	0.012	0.00372	140	44

Table 2. Model Parameters: The slow and fast muon production rates are from Braucher et al, 2011. The slow and fast attenuation lengths are from Braucher et al, 2003.

Parameter	Range/Value
Production Rate Fast Muons (atoms g ⁻¹)	0.039
Production Rate Slow Muons (atoms g ⁻¹)	0.012
Attenuation Length Fast Muons (g/cm ²)	5300
Attenuation Length Slow Muons (g/cm ²)	1737.2
¹⁰ Be Decay Constant	5.0 x 10 ⁻⁷
Sample Depth (meters)	0 to 110
Threshold Value (δ ¹⁸ O)	5.0-3.0
Concentration (atoms g-1 yr-1)	1000 to ~5000
Gamma Distribution Shape factor	0.1
Gamma Distribution Scale factor	(110 - depth)/2

Appendix:

A1. Determining sample depth below the surface

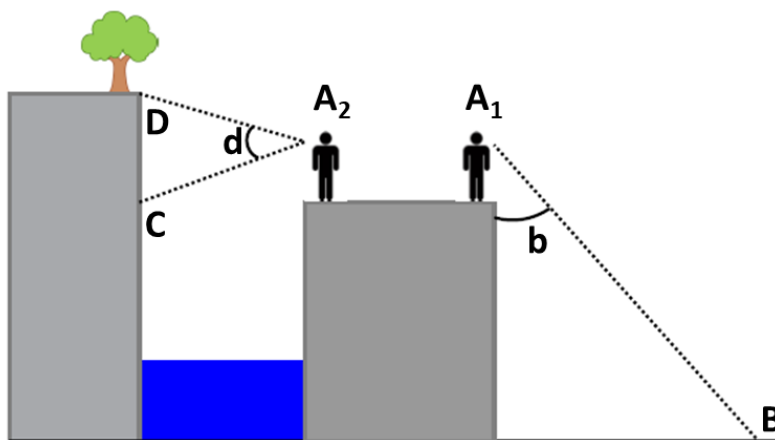
Historic USGS topographic maps, detailed in the table below, were selected using the following criteria: 1) the bounds of the map quadrangle must contain both the sampling site and a sufficient amount of the surrounding area such that an elevation is readable. 2) the year of the map survey must be pre-quarry or roadcut formation in order to determine the undisturbed surface elevation. Furthermore, while georeferencing was an inherent feature of the maps to insure accuracy each of the maps was compared with/checked against a satellite image base map in Arc GIS.

In order to determine the depth of the Oriskany Sandstone beneath the surface at each site the elevation of the Oriskany Sandstone needed to be measured. In the Hanson Quarries (Jamesville (Han1601), Skaneateles (Han1602), Oriskany Falls Lower Horizon (Han1603) and Oriskany Falls Upper Horizon (Han1604), the elevation of the Oriskany Sandstone was provided by quarry operators. In the remaining sampling sites, the Seneca Stone quarry (Seneca Stone) and the I88 Roadcut (I88S) a laser range finder, a device which uses a laser beam to measure the distance to an object and measures the inclination of the shot (laser), was used in order to measure the elevation of the Oriskany Sandstone (Appendix Figure 1).

Appendix Table 1. Historic USGS Topographic Map Details

Sample ID	Site Location	USGS Historical Topographic Map Quadrangle (Code)	Year	Scale	Contour Interval (m)
Seneca	Seneca Stone Corporation	Romulus, NY (136106)	1953	1:24000	3
Han1601	Hanson Aggregates Jamesville Quarry	Jamesville, NY (129988)	1973	1:24000	6
Han1602	Hanson Aggregates Skaneateles Quarry	Jordan, NY (130109)	1955	1:24000	3
Han1603	Hanson Aggregates Oriskany Falls Quarry (Lower horizon)	Oriskany Falls, NY (135895)	1943	1:24000	6
Han1604	Hanson Aggregates Oriskany Falls Quarry (Upper horizon)	Oriskany Falls, NY (135895)	1943	1:24000	6
I88S	Route I-88 Roadcut (Southern exposure)	Cobleskill, NY (137181)	1996	1:24000	6

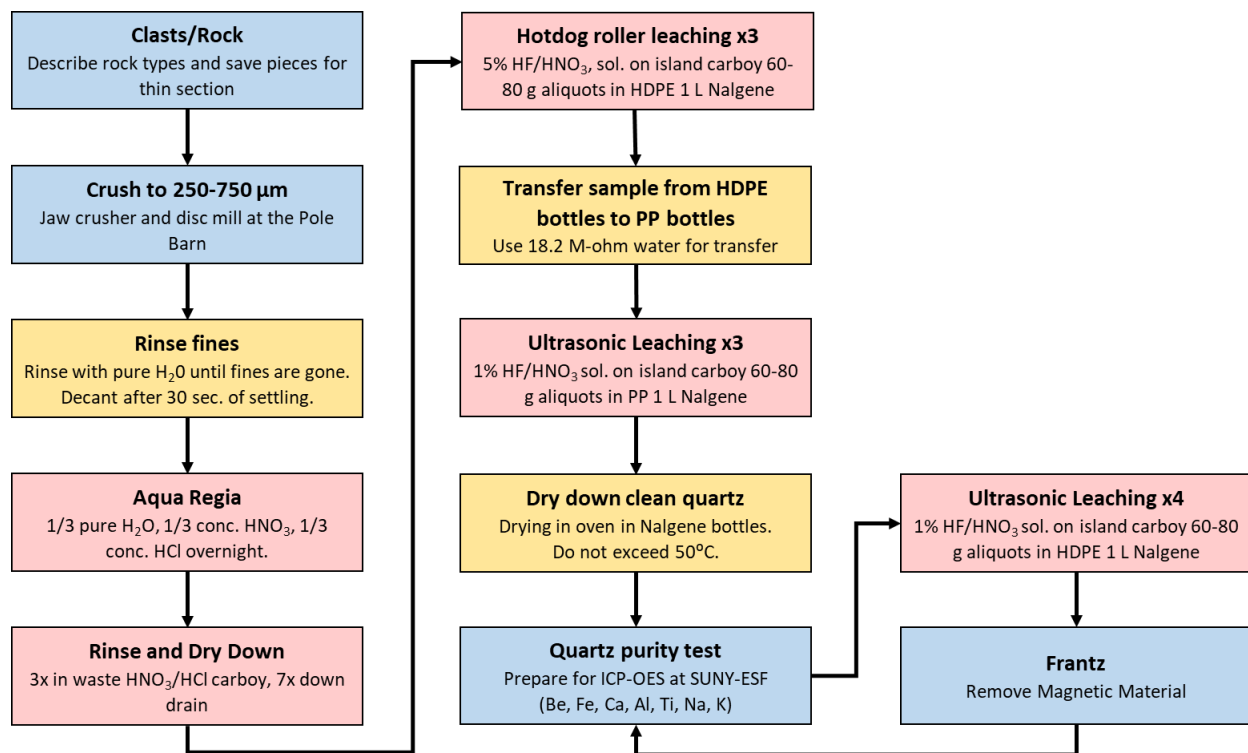
Appendix Figure 1. Laser Range Finder Diagram: The scenario in this figure mimics the methods used at the Seneca Stone quarry to measure the elevation of the Oriskany Sandstone. The first shot was from A_1 to B (Oriskany Sandstone), resulting in a measurement of the distance between those points and the inclination (b) of the shot. The height of the bench that point A_1 is on can be determined using the following equation. $Distance \times \sin(b) = Height$ To measure the full height of material above point B another measurement must be taken from point A_2 . This scenario allows for a different methodology which makes use of a built-in function of the laser range finder called the height routine. This routine uses two shots ($A_2 - D$ and $A_2 - C$) and the measured angle between them to determine the height of the wall with no secondary calculations needed.



A2. Sample processing

The process begins with sample collection, approximately 1kg of material at each site. Samples were crushed, using a rock hammer, jaw crusher and disc mill down to a target grain size between 250-750 μm , which was isolated using 750 and 250 μm sieves. The sieved sample was treated with aqua regia to remove carbonates. Leaching of silicate minerals occurred in two steps: 1) in a 5% HF/5% HNO₃ V/V solution in conjunction with agitation at 40°C using hotdog rollers and 2) in a 1% HF/1% HNO₃ in an ultrasonic bath at 40°C. The hotdog roller etching, and ultrasonic etching were initially repeated three times for each sample. Post etching, 250 mg of sample was dissolved in capped Teflon beakers with 5 ml of concentrated HF with 1% H₂SO₄ prior to fuming off the HF. The residual bead of H₂SO₄ was diluted with pure H₂O to assess quartz purity by measuring the concentrations of Be, Fe, Ca, Al, Ti, Na, K by Inductively Coupled Plasma Optical Emission Spectrometry (ICP-OES) at SUNY-ESF. Typical acceptable results are approximately 100 ppm of Al, < 100 ppm for Ti and Fe and < 30 ppm for Ca, Na and K, however quartzites typically have higher overall concentrations. The first quartz purity test (See Table 3) showed two of the samples still contained high concentrations. All samples were subject to an additional ultrasonic leaching and Han1603 and I88S had an additional 3 rounds of treatment. Finally, to remove additional non-quartz material the two “dirty” samples were run through the Frantz, a large electromagnet which separated magnetically susceptible minerals from the non-magnetically susceptible minerals. More specifically the samples were run through the Frantz 3x up to an amperage of 1.5. A follow-up quartz purity test showed an increase in purity in all the samples. Additional sample processing occurred at the University of Vermont following the procedures outlined in Corbett et al. (2016). For each sample 250 μg of ⁹Be carrier solution was added to 20 g of clean quartz and subsequently digested in HF at 135°C. After evaporating the HF, the sample was fumed 3x with perchloric acid at 230°C to remove fluorides.

Centrifuging the sample removed Ti and insoluble fluorides. ^{10}Be was then isolated by ion exchange chromatography (remove Fe, B, Ti) before being converted to BeO, mixed with Nb powder and packed into stainless steel cathodes for Accelerator Mass Spectrometry (AMS) analysis. AMS analysis was conducted at Purdue University's PRIME Lab.



Appendix Figure 2. Lab Protocols: Flowchart describing sample processing for quartz purification at Syracuse University.

Sample ID	Hotdog Roller Leaching	Ultrasonic Leaching	2 nd Ultrasonic Leaching	Frantz
Seneca Stone	3x	3x	1x	NA
Han1601	3x	3x	1x	NA
Han1602	3x	3x	1x	NA
Han1603	3x	3x	4x	3x to 1.5 amps
Han1604	3x	3x	1x	NA
I88S	3x	3x	4x	3x to 1.5 amps

Appendix Table 2. Syracuse University Sample Processing: The number of repetitions for each of the steps for each sample is listed here.

	Analyte Name and Concentration (ppm)												
Sample ID	Al 396.153	Al 308.215	Be 313.042	Ca 317.933	Ca 315.887	Fe 238.204	Fe 259.939	K 766.490	Mg 285.213	Mg 279.077	Na 589.592	Ti 334.940	Ti 336.121
Control	48.2	49.7	0.0	4.1	4.1	3.1	3.1	1.2	8.6	8.6	1.6	3.7	3.9
Seneca Stone	118.9	119.8	0.0	21.7	22.4	27.1	27.1	17.2	12.4	12.6	16.6	41.3	41.3
Han1601	138.1	139.5	0.0	17.3	17.1	28.6	28.5	16.9	11.2	11.4	17.0	47.3	47.6
Han1602	113.1	113.8	0.0	28.9	29.7	32.7	32.8	16.2	11.3	11.3	16.0	47.4	47.6
Han1603	137.8	144.5	0.0	539.7	535.5	172.9	172.6	33.3	19.0	18.6	33.4	41.6	41.6
Han1604	122.9	123.4	0.0	28.7	29.7	40.4	40.5	16.8	11.1	11.2	19.3	47.8	47.9
I88S	234.9	244.5	-0.1	54.4	53.7	87.3	87.2	32.4	32.0	31.6	29.3	237.2	238.9

Appendix Table 3. 1st Quartz Purity Results: In red are the analyte concentrations which are above the clean threshold, approximately 50 ppm for every analyte (excluding Al).

	Analyte Name and Concentration (ppm)												
Sample ID	Al 396.153	Al 308.215	Be 313.042	Ca 317.933	Ca 315.887	Fe 238.204	Fe 259.939	K 766.490	Mg 285.213	Mg 279.077	Na 589.592	Ti 334.940	Ti 336.121
Control	48.4	48.7	0.0	8.0	7.9	2.5	2.5	0.7	9.1	9.0	0.8	0.6	0.6
Seneca Stone	120.3	121.1	0.0	23.5	24.2	28.2	28.3	16.3	11.9	12.0	15.3	42.9	42.7
Han1601	129.1	130.2	0.0	16.8	16.5	30.6	30.6	15.1	10.8	10.9	15.1	45.7	45.7
Han1602	115.1	116.0	0.0	22.5	22.9	30.1	30.1	14.9	13.1	13.1	13.7	42.9	42.8
Han1603	132.0	138.8	0.0	482.2	479.6	162.5	162.4	32.4	18.1	17.6	30.1	42.6	42.5
Han1604	117.8	118.8	0.0	26.2	26.9	40.8	40.9	15.3	12.3	12.4	15.3	48.2	48.0
I88S	183.5	190.0	0.0	47.3	48.5	59.0	59.0	27.6	21.8	21.3	24.4	112.1	112.1

Appendix Table 4. 2st Quartz Purity Results: In red are the analyte concentrations which were above the clean threshold in the 1st test.

A3. Matlab forward modeling script (be aware that text wrapping truncates some lines)

```
function [median_depth, median_path, LR_t] = glacial_erosion_smooth3(s_depth, z,  
conc, unc)
```

```
%close all
```

```
%FUNCTION INPUTS
```

```
s_depth ;% Depth of sample collection (meters)
```

```
z ; % Elevation of quarry at Oriskany Falls
```

```
conc; % Concentration (atoms/g)
```

```
unc; % Concentration uncertainty
```

```
% MUON SCALING FACTORS
```

```
Ps1 = 1013.25; % Sea level pressure
```

```
gMR = 0.03417; % units = K m-1 (g is the acceleration due to gravity) % M is the molar  
weight of air and R is the ideal gas constant
```

```
Xi = 0.0065; % Adiabatic lapse rate (greek lower case Xi) = dT/dz = 0.0065 K m-1
```

```
Ts = 288.15; % Sea Level Temperature (units K)
```

```
Psite = (Ps1)*exp((-gMR/Xi)*(log(Ts)-log(Ts - Xi*z))); % Pressure as a function of  
elevation
```

```
Sf = exp((1013 - Psite)/260); %Scaling factor for fast muons
```

```
Ss = exp((1013- Psite)/510); %Scaling factor for slow muons
```

```
% MUON PRODUCTION RATE (Braucher et al, 2011)
```

```
P10Be_f= 0.039*Sf; % Fast muons
```

```
P10Be_s = 0.012*Ss; % Slow muons
```

```
% MUON DEPTH DEPENDENT PARAMETERS (Braucher, 2003)
```

```
atten_leng1 = ((736.6 + 2688)/2); % Attenuation length (cm2/g); slow muon
```

```
atten_leng2 = 5300; % Attenuation length (cm2/g); fast muon
```

```
Rho = 2.25; % g/cm3density of the overburden
```

```
Mu1 = (Rho/atten_leng1); % Slow
```

```
Mu2 = (Rho/atten_leng2); % Fast
```

```
%ADDITIONAL PARAMETERS
```

```
lambda_Be = 5.0e-07; (Chmeleff, 2010; Korschinek, 2010) %Lambda = Decay Constant
```

```
lambda_Al = 9.83e-07; (Norris et. al., 1983)
```

```
E = 0; % Epsilon/Erosion
```

```
E1 = 0.0025; %Background Erosion Rate for the NE US (initial condition) (cm/yr)  
(Matmon et al., 2003a; Matmon et al., 2003b; Reuters, 2003)
```

```
%TIME AND ICE COVER
```

```
%Lisiecki and Raymo 2005 d18O record (last Ma).
```

```
load('LR04_stack');
```

```
n = length(LR04stack);
```

```
for i = 3:n-3
```

```
    boxcar(i) = mean(LR04stack(i-2:i+2,2));
```

```
end
```

```
for i = 3:n-3
```

```
    LR04stack(i,2) = transpose(boxcar(i));
```

```
end
```

```
B = LR04stack;
```

```
Ma = find(LR04stack(:,1) == 1000);
```

```
B = flipud(B(1:Ma,:));
```

```
LR_t = B(:,1)*1000; %Time (ka)
```

```
LR_d18O = B(:,2); %Benthic d18O (per mil)
```

```
LR_uncert = B(:,3); %Standard error (per mil)
```

```
%Set a d18O threshold value >ice sheet cover, <ice free conditions
```

```
%Conservative estimate based on timing of LGM retreat from this latitude
```

```
%(Use the d18O value from retreat)
```

```
Th_d18O = 4.8; %threshold value for d18O, If d18O value is greater than P10Be is zero
```

```
f_c = LR_d18O;
Th(f_c>4.8) = 0;
Th(f_c<=4.8) = 1;
Th = Th';
```

%CHANGE IN DEPTH THROUGH TIME

```
%Determining the number of glacial events in the window of time (based on
%Lisiecki and Raymo threshold)
%index = zeros(1,11); % is referring to the number of glacial events (g_e_num)
j = 1;
for i = 2:801
    g_events(i) = ((Th(i) - Th(i-1)) == 1);
    if g_events(i) == 1
        index(j) = i;
        j = j+1;
    end
end
end
```

```
g_e_num = sum(g_events); %Number of glacial events
```

%GAMMA DISTRIBUTION

```
b = ((Mu2^-1*.05) - s_depth)/2; % Scale parameter for gamma distribution
a = 0.1; % Shape parameter for gamma distribution
```

```
n = 10000; % NUMBER OF SIMULATIONS
```

```
e_events = zeros(g_e_num,n); % creates empty matrix of erosion events
```

```
%gamrnd: generates random numbers from the gamma distribution with shape
%parameters in A and scale parameter in B. A and B can be vectors,
%matrices, or multidimensional arrays that all have the same size.
%A scalar input for A or B is expanded to a constant array with the same
%dimensions as the other input.
```

```

for i = 1:n;

    e_events(:,i) = gamrnd(a,b,g_e_num,1);
    while sum(e_events(:,i)) > (b*2);
        e_events(:,i) = gamrnd(a,b,g_e_num,1); %e_vents = 10000 possible chnages in
depth synced with the g_e_num
    end
end

%total amount of erosion for each of the 10000 modeled scenarios
tot_er = sum(e_events);

%Starting depth
X1 = tot_er + s_depth+E1*.01*LR_t(1);
%Final depth is equal to sample depth
XF = s_depth;
e_events2 = [X1;e_events]; %First row of e_events2 is now the starting depth
dtt = e_events2; %dtt = depth through time

%This loop subtracts the erosion events from the starting depth, so after
%the last erosion event the depth is the sample depth (s_depth)
w = (g_e_num + 1);
for k = 1:n
    for j = 2:w
        dtt(j,k) = e_events2(1,k) - sum((e_events2(2:j,k)));
    end
end

%e_events indexed to match g_events; sets the timing of the changes in depth
depths = zeros(Ma,n);
index = [1 index];
for k = 1:n
    depths(index,k) = dtt(:,k);
end

```

```

end

for i =1:(numel(index)-1);
    for j = 1:n;
depths(((index(i)):(index(i+1)-1)),j) = depths(index(i),j);
    end
end

%add background erosion of surface
t_int = LR_t(1:Ma-1) - LR_t(2:Ma);
t_int = [0; t_int];
e_int = cumsum(t_int*E1*.01);

%e_int2 = ones(Ma,n);
for j = 1:n;
    for i = 2:Ma
        depths(i,j) = depths(i,j)-e_int(i);
    end
end

%depths = depths+e_int2;

depths(786:801,1:10000) = s_depth;
depths = depths*100;

%Calculate production as a function of ice free and ice covered time
%periods

%PRODUCTION (through time with changing depth)

%Set initial inherited concentration based on start depth
N_10Be_slow = zeros(Ma,n);
N_10Be_fast = zeros(Ma,n);

```

```

for k = 1:10000
N_10Be_slow(1,k) = ((P10Be_s)/(lambda_Be + Mu1*E1))*exp(-depths(1,k)*Mu1);
N_10Be_fast(1,k) = ((P10Be_f)/(lambda_Be + Mu2*E1))*exp(-depths(1,k)*Mu2);
end

% Calculate the time evolution of concentration

for i = 2:801;
for j = 1:10000;
    N_10Be_slow(i,j) = N_10Be_slow(i-1,j)*(exp(-lambda_Be*(LR_t(i-1)-
LR_t(i))))+Th(i)*((P10Be_s)/(lambda_Be + Mu1*E1))*exp(-depths(i,j)*Mu1)*(1 - exp(-
(lambda_Be + Mu1*E1)*(LR_t(i-1)-LR_t(i))));
N_10Be_fast(i,j) = N_10Be_fast(i-1,j)*(exp(-lambda_Be*(LR_t(i-1)-
LR_t(i))))+Th(i)*((P10Be_f)/(lambda_Be + Mu2*E1))*exp(-depths(i,j)*Mu2)*(1 - exp(-
(lambda_Be + Mu2*E1)*(LR_t(i-1)-LR_t(i))));
end
end

%Sum fast and slow muon production
N_tot_Be = N_10Be_slow + N_10Be_fast;

%Find solutions that fit observed value +/- 1-sigma
R = find(N_tot_Be(801,:)<conc+unc & N_tot_Be(801,:)>conc-unc);

%calculate the mean, mean and standard deviation of all acceptable fits for
%concentrations AND
mean_path = mean((N_tot_Be(:,R))');
std_path = std((N_tot_Be(:,R))');
median_path = median((N_tot_Be(:,R))');

depths_m = depths/100;
mean_depth = mean((depths_m(:,R))');
std_depth = std((depths_m(:,R))');

```

```

median_depth = median((depths_m(:,R)));

% Plotting

%selected
LR_t2 = 1000000-LR_t; % fixed LR timeline for plotting on these figures

figure(1) % Time vs. Concentration
subplot(2,1,1)
plot(LR_t,N_tot_Be,'LineWidth',0.25,'color',[0 0 0]+0.75)
title('Simulations')
hold on
plot(LR_t,N_tot_Be(:,R),'Linewidth',0.25,'color','r')
hold on
plot(LR_t,median_path,'y','LineWidth',4)
hold off
title('Simulations')
set(gca,'FontSize',15)
ylabel('[10Be] atoms/g')
set(gca,'FontSize',15)
xlabel('Time (100,000 years)')
set(gca,'FontSize',15)
set(gca, 'XTicklabel', [0 1 2 3 4 5 6 7 8 9 10 ])
set(gca,'FontSize',15)
set(gca,'XDir','Reverse')
hold on
scatter(0,conc,'filled','k')

subplot(2,1,2) %Time vs. Depth
[hAx,hLine1,hLine2] = plotyy(LR_t,depths_m,LR_t2,LR_d18O); % All simulations
ylabel(hAx(1),'Depth Below the Surface (m)','FontSize',15,'color','k') % Left y-axis
ylabel(hAx(2),'Benthic \delta18O(‰)','FontSize',15,'color','b') % Right y-axis
set(hLine1,'LineWidth',0.25);

```



```

set(hLine1,'Color',[0 0 0]+0.75);
set(hLine2,'LineWidth',2);
set(hLine2,'Color','b');
set(hAx(2),'ycolor','b','fontsize',15)
hold on
plot(LR_t,depths_m(:,R),'r','LineWidth',0.25)% Select simulations
hold on
plot(LR_t,median_depth,'y','LineWidth',4)% Median simulation
xlabel('Time (100,000 years)')
set(gca,'FontSize',15)
set(gca, 'XTicklabel', [0 1 2 3 4 5 6 7 8 9 10 ])
set(gca,'YDir','Reverse')
set(gca,'FontSize',15)
set(gca,'XDir','Reverse')

figure(2)
subplot(2,1,2)
[hAx,hLine1,hLine2] = plotyy(LR_t,median_depth,LR_t2,LR_d18O); %all simulations
ylabel(hAx(1),'Depth Below the Surface (m)','FontSize',15,'color','k') % left y-axis
ylabel(hAx(2),'Benthic \delta18O(‰)','FontSize',15,'color','b') % right y-axis
set(hLine1,'LineWidth',3);
set(hLine1,'Color','b');
set(hLine2,'LineWidth',2);
set(hLine2,'Color','b');
set(hAx(2),'ycolor','b','fontsize',15)
set(hAx(1),'ycolor','r','fontsize',15)
xlabel('Time (100,000 years)')
set(gca,'FontSize',15)
set(gca, 'XTicklabel', [0 1 2 3 4 5 6 7 8 9 10 ])
set(gca,'YDir','Reverse')
set(gca,'FontSize',15)
set(gca,'XDir','Reverse')

```

```

subplot(2,1,1)
plot(LR_t,median_path,'r','LineWidth',4)
hold off
title('Simulations')
set(gca,'FontSize',15)
ylabel('[10Be] atoms/g')
set(gca,'FontSize',15)
xlabel('Time (100,000 years)')
set(gca,'FontSize',15)
set(gca, 'XTicklabel', [0 1 2 3 4 5 6 7 8 9 10 ])
set(gca,'FontSize',15)
set(gca,'XDir','Reverse')
%scatter(0,conc,'filled','k')

%P10Be_f= 0.039;%fast_muons
%P10Be_s = 0.012;%slow muons
rho_unc = 0.225;
P_unc_f = 0.004;
P_unc_s = 0.012;
hl = 1.38;
hl_unc = 0.018;
mu_unc_f = 950;
mu_unc_s = 171.23;

P_tot = P10Be_f + P10Be_s;

D_cm = (s_depth*100);
weight_total =(P10Be_f*exp(-D_cm*Mu2))+(P10Be_s*exp(-D_cm*Mu1));
weight_f = (P10Be_f*exp(-D_cm*Mu2))/weight_total;
weight_s = (P10Be_s*exp(-D_cm*Mu1))/weight_total;
P10Be_f2 = 0.039;

```

%Age and Erosion Rate Calculations (with uncertainty)

$$\text{Age} = -1/\lambda_{\text{Be}} \cdot \log\left(1 - \frac{\lambda_{\text{Be}} \cdot \text{conc}}{\left(\text{P10Be}_f \cdot \exp\left(-D_{\text{cm}} \cdot \mu_2\right) + \text{P10Be}_s \cdot \exp\left(-D_{\text{cm}} \cdot \mu_1\right)\right)}\right)$$

Age_unc =

$$\text{Age_unc} = \sqrt{\left(\frac{\text{hl_unc}}{\text{hl}}\right)^2 + \left(\frac{\text{P_unc}_f/\text{P10Be}_f}{\text{weight}_f}\right)^2 + \left(\frac{\text{P_unc}_s/\text{P10Be}_s}{\text{weight}_s}\right)^2 + \left(\frac{\text{unc}}{\text{conc}}\right)^2}$$

$$\text{E_rate} = \left(\frac{1}{\text{Rho}/\text{atten_leng2}}\right) \cdot \left(\frac{\text{P10Be}_f \cdot \exp\left(-D_{\text{cm}} \cdot \mu_2\right)}{\text{conc}} - \lambda_{\text{Be}}\right)$$

E_rate_unc =

$$\text{E_rate_unc} = \sqrt{\left(\frac{\text{rho_unc}}{\text{Rho}}\right)^2 + \left(\frac{\mu_{\text{unc}}_f/\text{atten_leng2}}{\text{weight}_f}\right)^2 + \left(\frac{\mu_{\text{unc}}_s/\text{atten_leng1}}{\text{weight}_s}\right)^2 + \left(\frac{\text{hl_unc}}{\text{hl}}\right)^2 + \left(\frac{\text{P_unc}_f/\text{P10Be}_f}{\text{weight}_f}\right)^2 + \left(\frac{\text{P_unc}_s/\text{P10Be}_s}{\text{weight}_s}\right)^2 + \left(\frac{\text{unc}}{\text{conc}}\right)^2}$$

References

- Abe-Ouchi, A., Saito, F., Kawamura, K., Raymo, M.E., Okuno, J., Takahashi, K. and Blatter, H., 2013, Insolation-driven 100,000-year glacial cycles and hysteresis of ice-sheet volume: *Nature*, v. 500, p. 190-193.
- Anderson, E.J., and Goodwin, P.W., 1991, PAC Stratigraphy of the Helderberg Group: Cycle Definition, Allogenic Surfaces, Hierarchy, Correlation and Relationship to "Vail" Sequences: *New York State Geological Association 63rd Annual Meeting Field Trip Guidebook*, p. 119-130.
- Anderson, R.S., and Anderson, S.P., 2010, *Geomorphology: The Mechanics and Chemistry of Landscapes*. Cambridge University Press,
- Balco, G., 2011, Contributions and unrealized potential contributions of cosmogenic-nuclide exposure dating to glacier chronology: *Quaternary Science Reviews*, p. 1990–2010, v. 30, (1-2), 3–27. <http://doi.org/10.1016/j.quascirev.2010.11.003>
- Balco, G., and Rovey C.W., 2010, Absolute Chronology for Major Pleistocene Advances of the Laurentide Ice Sheet: *Geology*, v. 38.9, p. 795-798.
- Bierman, P.R., Marsella, K.A., Patterson, C., Davis, P.T., and Caffee, M., 1999, Mid-Pleistocene cosmogenic minimum-age limits for pre-Wisconsinan glacial surfaces in southwestern Minnesota and southern Baffin Island; a multiple nuclide approach: *Geomorphology*, v. 27, p. 25-39.
- Bierman, P. R., Davis P.T., Corbett L.B., Lifton, N.A, Finkel R.C., 2015, Cold-based Laurentide ice covered New England's highest summits during the Last Glacial Maximum: *Geology*, v.43, no. 12, p. 1059-1062.

- Bloom, A.L., 2004, The Finger Lakes: a longer look: Geological Society of America Abstracts with Programs, Vol. 36, No. 2, p. 94.
- Braucher, R., Brown, E.T., Bourlés, D.L., Colin, F., 2003, In situ produced ^{10}Be measurements at great depths: implications for production rates by fast muons: Earth and Planetary Science Letters, v. 211, p. 251-258.
- Braucher, R., Merchel, S., Borgomano, J., Bourlés, D.L., 2011, Production of cosmogenic radionuclides at great depth: A multi element approach: Earth and Planetary Science Letters, v. 309, p. 1-9.
- Brigham, A.P., 1893, The Finger Lakes of New York: American Geographical Society, v. 25, no.1, p. 203-223
- Briner, J., Miller, G., Davis, P., Bierman, P., Caffee, M., 2003. Last Glacial Maximum ice sheet dynamics in Arctic Canada inferred from young erratics perched on ancient tors. Quaternary Science Review, v. 22, p. 437–444.
- Chmeleff, J., von Blanckenburg, F., Kossert, K., and Jakob, D., 2010, Determination of the ^{10}Be half-life by multicollector ICP-MS and liquid scintillation counting: Nuclear Instruments and Methods in Physics Research Section B: Beam Interactions with Materials and Atoms, v. 268.2, p. 192-99.
- Corbett, L.B., Bierman, P.R., Rood, D.H., 2016, An approach for optimizing in situ cosmogenic ^{10}Be sample preparation: Quaternary Geochronology, p. 24-34, v. 33.
- Davis, P.T., Bierman, P.R., Marsella, K.A., Caffee, M.W., Southon, J.R., 1999, Cosmogenic analysis of glacial terrains in the eastern Canadian Arctic: a test for inherited nuclides and the effectiveness of glacial erosion: Annals of Glaciological Society, v. 28, p. 181-188.

- Delmas, M., Calvet, M., Gunnell, Y., 2009, Variability of Quaternary glacial erosion rates – A global perspective with special reference to the Eastern Pyrenees: *Quaternary Science Reviews*, v. 28, p. 484-498
- Dunai, T.J., 2010, *Cosmogenic Nuclides: Principles, Concepts and Applications in the Earth Surface Sciences*: Cambridge University Press, p. 5.
- Dunai, T. J., and Lifton. N. A., 2014, The Nuts and Bolts of Cosmogenic Nuclide Production: *Elements*, v. 10.5, p. 347-50.
- Fisher, D. W., Isachen, Y. W., Rickard, L. V., 1970, New York State Museum and Science Service Map and Chart Series NO. 15.
- Friedlander, M. W., 1989, *Cosmic Rays*: Harvard University Press, Cambridge, Mass.
- Fullerton, D. S., 1986, Stratigraphy and Correlation of Glacial Deposits from Indiana to New York and New Jersey: *Quaternary Science Reviews*, v. 5, p. 23–37.
- Gray, L.M., Paleocology, Origin, and Significance of a Shell-Rich Bed in the Lowermost Part of the Ludlowville Formation (Middle Devonian, Central New York), 1991, *Dynamic Stratigraphy and Depositional Environments of the Hamilton Group (Middle Devonian) in New York State*. Ed. Carlton E. Brett and Ed Landing. Albany, NY: University of the State of New York, State Education Dept.
- Gosse, J.C., and Phillips, F.M.. 2001, Terrestrial in Situ Cosmogenic Nuclides: Theory and Application: *Quaternary Science Reviews* 20.14, p. 1475-1560.
- Granger, D. E., Lifton, N. A., & Willenbring, J. K. (2013). A cosmic trip: 25 years of cosmogenic nuclides in geology. *Geological Society of America Bulletin*, 125(9-10), 1379–1402. <http://doi.org/10.1130/B30774.1>

- Kehew, A.E., Lord, M.L., Kozlowski, A.L., Fisher, T.G., 2009, Megaflooding on Earth and Mars: Proglacial megaflooding along the margins of the Laurentide Ice Sheet: Cambridge, Cambridge University Press, p. 104-127.
- Korschinek, G., Bergmaier, A., Faestermann, T., Gerstmann, U.C., Knie, K., Rugel, G., Wallner, A., Dillmann, I., Dollinger, G., Lierse von Gostomski, Ch., Kossert, K., Maiti, M., Poutivtsev, M., and Remmert, A., 2010, A new value for the half-life of ^{10}Be by Heavy-Ion Elastic Recoil Detection and liquid scintillation counting: Nuclear Instruments and Methods in Physics Research Section B: Beam Interactions with Materials and Atoms, v. 268.2, p. 187-91.
- Lal, D., 1991, Cosmic Ray Labeling of Erosion Surfaces: In Situ Nuclide Production Rates and Erosion Models: Earth and Planetary Science Letters, 104.2-4, p. 424-39.
- Lifton, N., Sato, T., Dunai, T., 2014, Scaling in situ cosmogenic nuclide production rates using analytical approximations to atmospheric cosmic-ray fluxes: Earth and Planetary Science Letters, v. 386, p. 149–160
- Lisiecki, L.E., Raymo, M.E., 2005, A Pliocene-Pleistocene stack of 57 globally distributed benthic D18O records: Paleoceanography, v. 20, p. 1-17
- MacClintock, P., and Apfel, E. T., 1944, Correlation of the Drifts of the Salamanca Re-Entrant, New York: Geological Society of America Bulletin, v. 55, no. 10, p. 1143–1164.
- Matmon, A., Bierman, P.R., Larsen, J., Southworth, S., Pavich, M., and Caffee, M., 2003a, Temporally and spatially uniform rates of erosion in the southern Appalachian Great Smoky Mountains: Geology, v. 31, p. 155-158.

- Matmon, A.S., Bierman, P., Larsen, J., Southworth, S., Pavich, M., Finkel, R., and Caffee, M., 2003b, Erosion of an ancient mountain range, the Great Smoky Mountains, North Carolina and Tennessee: *American Journal of Science*, v. 303, p. 817-855.
- Muller, E. H., 1977, Late Glacial And Early Postglacial Environments In Western New York: *Annals of the New York Academy of Sciences*, v. 288, no. 1, p. 223–233.
- Muller, E. H., and Calkin P. E., 1993, Timing of Pleistocene Glacial Events in New York State: *Canadian Journal of Earth Sciences*, v. 30.9, p. 1829-845.
- Mullins, H.T., Hinchey E.J., Wellner R.W., Stephens D.B., Anderson W.T., Dwyer T.R., and Hine A.C., 1996, Seismic Stratigraphy of the Finger Lakes: A Continental Record of Heinrich Event H-1 and Laurentide Ice Sheet Instability, *Geological Society of America: Special Paper 311: Subsurface Geologic Investigations of New York Finger Lakes: Implications for Late Quaternary Deglaciation and Environmental Change*, p. 1-35.
- Norris, T. L., Gancarz A. J., Rokop D.J., and Thomas K.W., 1983, Half-life of ^{26}Al : *Journal of Geophysical Research* v. 88, p. B331–B333.
- Oliver, W., DeWitt, W., Dennison J., Hoskins D., Huddle J., 1967, Devonian of the Appalachian basin, United States, in *International Symposium on the Devonian System*, V. 1, Alberta Soc. Petroleum Geologists, Calgary, 1001.
- Paillard, D., 1998, The timing of Pleistocene glaciations from a simple multiple-state climate model: *Nature*, v.391, p. 378-381.
- Phillips, F.M., Argento, D.C., Balco, G., Caffee, M.W., Clem, J., Dunai, T.J., Finkel, R., Goehring, B., Gosse, J.C., Hudson, A.M., Jull, A.J.T., Kelly, M.A., Kurz, M., Lal, D., Lifton, N., Marrero, S.M., Nishiizumi, K., Reedy, R.C., Schaefer, J., Stone, J.O.H., Swanson, T.,

- Zreda, M.G., 2016, The CRONUS-Earth Project: A synthesis: *Quaternary Geology*, v. 31, p. 119-154.
- Reuter, J., Bierman, P.R., Pavich, M., Gellis, A., Larsen, J., and Finkel, R., 2003, Long-term sediment generation rates derived from ^{10}Be in river sediment of the Susquehanna River Basin, in "channeling through time: Landscape evolution, land use change, and stream restoration in the lower Susquehanna Basin", in Merritts, D., Walter, R., and de Wet, A., eds., *Southeastern Friends of the Pleistocene Fall 2003 Guidebook*, p. 48-55.
- Rogers, W.B., Isachen, Y.W., Mock, T.D., and Nyahay, R.E., 1990, *New York State Geological Highway Map: Educational Leaflet 33*
- Ryder, R. T., 1995, Appalachian Basin Province (067), in Gautier, D. L., Dolton, G.L., Takahashi, K.I., and Varnes, K.L., ed., 1995 National assessment of United States oil and gas resources--Results, methodology, and supporting data: U.S. Geological Survey Digital Data Series DDS-30, Release 2, one CD-ROM, 144 p., 28 figures, one CD-ROM.
- Selleck, B., 2010, *Stratigraphy of the Northern Appalachian Basin, Mohawk Valley, Central New York State: Department of Geology, Colgate University.*
- Sharma, P., and Middleton, R., 1989, Radiogenic production of ^{10}Be and ^{26}Al in uranium and thorium ores: Implications for studying terrestrial samples containing low levels of ^{10}Be and ^{26}Al : *Geochimica et Cosmochimica Acta*, v 53.3, p. 709-716.
- Snyder, Kent E., and Ray B. Bryant, 1992, *Late Pleistocene Surficial Stratigraphy and Landscape Development in the Salamanca Re-entrant, Southwestern New York: Geological Society of America*, 104, p. 242-251.

Stroeven, A. P., Fabel, D., Hattestrand, C., and Harbor, J., 2002, A relict landscape in the centre of Fennoscandian glaciation: cosmogenic radionuclide evidence of tors preserved through multiple glacial cycles: *Geomorphology*, v. 44, p. 145-154.

Tarr, R.S., 1893, Lake Cayuga a Rock Basin: *Geological Society of America Bulletin*, v. 5, p. 339–356.

Tarr, R.S., 1902, *The physical geography of New York state*. (p. 1–435). New York: MacMillian.

Valletta, R. D., Willenbring, J. K., & Lewis, A. R., 2017, “Difference Dating”: A novel approach towards dating alpine glacial moraines: *Quaternary Geochronology*, v. 41, p. 1–10.
<http://doi.org/10.1016/j.quageo.2017.05.001>

von Engel, O.D., 1961, *The Finger Lakes region: its origin and nature*: Ithaca, NY, Cornell University Press, p. 156.

Curriculum Vitae

JENNIFER NAIR

EDUCATION

M.S. in Earth Sciences - GPA: 3.41 Aug 2018
Syracuse University, College of Arts & Sciences, Syracuse, NY
Thesis: Non-uniform glacial erosion in New York State viewed through the lens of cosmogenic nuclide concentrations and forward modeling

B.S. in Environmental Science - GPA: 3.64 Dec 2014
Emory University, Emory College of Arts & Sciences, Atlanta, GA

EMPLOYMENT

Teaching Assistant, Department of Earth Sciences, Syracuse University 2015 - 2018
Recitations and lab sections for: Climate Change: Past & Present, Earth System Science, Earth Science, Volcanoes & Earthquakes

RESEARCH EXPERIENCE

Awarded \$2,500 through the Nelson and Prucha Graduate Research Funds May 2016
Project: Sculpting the Finger Lakes and exploring the smooth-rough transition south of the Valley Heads Moraine

Independent research at the Michael C. Carlos Museum, Emory University May-Aug 2014
Project: Non-destructive methods (stereomicroscope properties, specific gravity and index of refraction) in identifying and classifying carved gem minerals used in ancient glyptic art

PRESENTATIONS

Central New York Earth Science Student Symposium (CNYESS) Apr 2018
Oral presentation: Variable Glaciated Topography of New York State: Erosion through the lens of Cosmogenic Nuclide Concentrations and Forward Modeling

Central New York Earth Science Student Symposium (CNYESS) Apr 2017
Poster presentation: Glacial control of topography in New York State: inferences from cosmogenic nuclide concentrations

LEADERSHIP EXPERIENCE

Treasurer of the Geology Graduate Organization (GeoGo) 2016 - 2018

TECHNICAL SKILLS

Software: MATLAB and ArcGIS
Rock sample preparation for mineral separation and isolation of quartz using chemical leaching